5-2018

Modeling Impacts of Light Absorbing Particles on Glacial Melt and Albedo: Construction, Quantified Impacts, and Simulations from the Cordillera Blanca, Peru

Bria Riggs
Bates College, briggs@bates.edu

Modeling Impacts of Light Absorbing Particles on Glacial Melt and Albedo: Construction, Quantified Impacts, and Simulations from the Cordillera Blanca, Peru

A Senior Thesis

Presented to

The Faculty of the Program of Environmental Studies

Bates College

In partial fulfillment of the requirements for the

Degree of Bachelor of Arts

By

Bria Riggs

Lewiston, Maine

April 13, 2018

1. Acknowledgements

First I want to thank my parents, Julie Winn and Dave Riggs, for supporting me in my expedition to Peru and my academic pursuits over the past many years. Next, thank you as big as the mountains of the Cordillera Blanca to my advisors, Holly Ewing and Carl Schmitt, without whom this thesis would not be a reality. Thank you to John All, Ellen Lapham, and the rest of the American Climber Science Program for accepting me onto their research team to share adventures in science and mountaineering. A very special thank you to Chris Stevens, Jeff Pratt, Matt Lubar, Sam Kaiser, Janae Gallant, Niki Alden, and Gina Heuscher for being fast friends, stellar climbing buddies, and willing to help me carry many kilograms of snow samples down from the mountain tops. To Danielle, Halley, Sarah, Dylan, Sadie Mae and the rest of my second family here at Bates, thank you for your endless support and solidarity in the classroom, library, and beyond. Finalmente, muchisimas gracias a Joaquin, Joel, Francisco, Nemo, Chris, y toda de la gente en Peru por su generosidad y por compartir su país y sus montañas conmigo, esta tesis es para ustedes.

2. **Table of Contents**

3. List of Figures

4. List of Tables

5. Abstract

Glaciers act as important water storage units that supply both human and ecological communities. However, glacial systems are threatened by rising global temperatures as well as light absorbing particles (LAPs) on the surface and within the snowpack that increase energy absorption and decrease albedo. The majority of hydrological models used to examine glacial melt at the watershed level assume a constant albedo of 0.75 for all snow surfaces. This assumption neglects the impact that LAPs have on albedo, energy processes, and melt rates. Additionally, current models used to simulate changes in albedo due to LAPs do not separate the impacts of LAPs on the surface and LAPs within the snowpack. The model presented in this study aims to separate the impacts of LAPs on the surface, LAPs within the snowpack, and temperature on melt and albedo within the glacial snowpack system. Scenarios aimed at quantifying such impacts as well as identifying the behavior of the model within specified input ranges were run using experimental data. The concentration of LAPs in the snowpack had the greatest impact on all output variables from the model. Additionally, simulations of LAP accumulation at the col and summit of Pisco in the Cordillera Blanca, Peru were run in order to compare model outputs with raw field data. The model produced simulated LAP concentrations within ±22.1 ng g^{-1} of the measured value at the col and ±0.01 ng g^{-1} at the summit. Finally, scenarios were run in order to simulate towers created through anthropogenic tampering of the surface albedo. The model produced simulated tower heights of up to 2.5 meters. This model may be constructed further in order to be integrated into a larger hydrological model, which could have broad implications for the impact of glacial melt due to LAPs within watershed systems.

6. Introduction

Glaciers around the world are currently experiencing drastic changes due to rising global temperatures. As important water storage units, accelerated glacial melt threatens both ecological and human communities. In addition to rising temperatures, glacier mass balance is impacted by inputs of light absorbing particles (LAPs) to the system. Through processes of atmospheric deposition, LAPs such as black carbon (BC) and dust, originating from both natural and anthropogenic sources, impact the structure and processes of the cryosphere (Marshall 2012).

LAPs collect both on the surface and within the snowpack, thus reducing albedo and adding energy to the glacial system, which increases melt rates (Aoki et al. 2011, Goelles and Bøggild 2017, Khan et al. 2017) (Figure 1). While the impact of rising global temperatures on glacial melt has been widely studied around the world, the impact of LAPs on melt processes has become a more prominent field of study in recent years (Oerlemans and Fortuin 1992, Barnett et al. 2005, Pellicciotti et al. 2005, Flanner et al. 2007). Studies using in-situ data have focused on the impacts of LAPs in specfic regions of the world, namely Greenland, the poles, and the Himalaya (Babu et al. 2011, Ginot et al. 2014, Kaspari et al. 2014, Khan et al. 2017, Thomas et al. 2017).

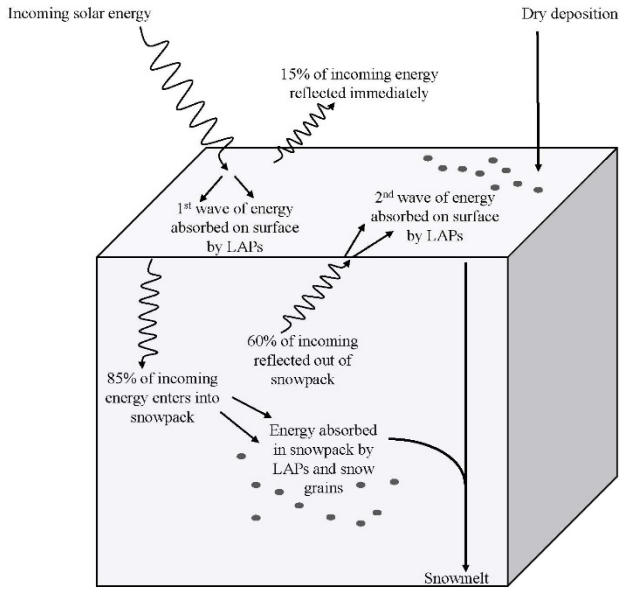

Figure 1: Conceptual model of snowpack energy processes and the function of LAPs in the system.

In addition to utilizing in-situ data to investigate the impacts of temperature and LAPs within specific areas, models have also been developed to predict future changes in glacial systems (Aoki et al. 2011, Hadley and Kirchstetter 2012). Ablation and mass balance modelling are often structured with an energy balance or temperature-index approach (Anderson 1968, Meador and Weaver 1980, Braithwaite 1981, Kustas et al. 1994, Hock 2003, Senese et al. 2014). Hock et al. (2003) developed a temperature-index model, based on degree days, to investigate snow and ice melt specifically within mountain environments. Braithwaite (1981) developed a model to investigate the relationship between energy balance, ablation, and temperature in glacial systems. Other ablation models have been developed using an energy balance framework, which utilizes radiation data in order to model energy fluxes and ablation in and on the glacier(Anderson 1968, Kustas et al. 1994). Kustas et al. (1994) tested degree-day and restricted degree-day, both temperature-index based approaches, and an energy balance approach in order to reconcile the different modelling foundations for ablation and produce more accurate snowmelt estimates. While it was found that the restricted degree-day approach produced estimates most closely related to data taken from a stream gauge, the study also concluded that the estimates could be improved by coupling the restricted degree-day model with an energy budget model (Kustas et al. 1994).

While a subset of these models account for energy absorption by LAPs, the additional energy absorption is accounted for within the snowpack and not on the surface of the snow, despite LAPs congregating both within the snowpack and on the surface. The Snow, Ice, and Aerosol Radiative (SNICAR) model, developed by Flanner and Zender (2005, 2007) is based on theory from Wiscombe and Warren (1980) and the two-stream radiative approximation

used by Toon et al. (1989) to estimate broadband albedo values. Various types of LAPs, each scaled by their different absorptive properties, can be integrated into the model in order to account for the impact of LAPs on albedo (Flanner and Zender 2005).

Despite the implementation of models in various locations around the world to estimate ablation due to LAPs and/or temperature, there are no existing models that separate the impact of LAPs within the snowpack, LAPs on the snow surface, and air temperatures on snowpack energetics, albedo, and melt processes. The purpose of this study is to present a model that integrates both the surface energy balance and temperature-index approaches to modeling in order to identify the conditions in which snowmelt is driven by (a) LAPs on the snow surface, (b) LAPs within the snowpack, or (c) air temperature. Experimental data are used to examine model behavior the model while raw data are used to simulate conditions at

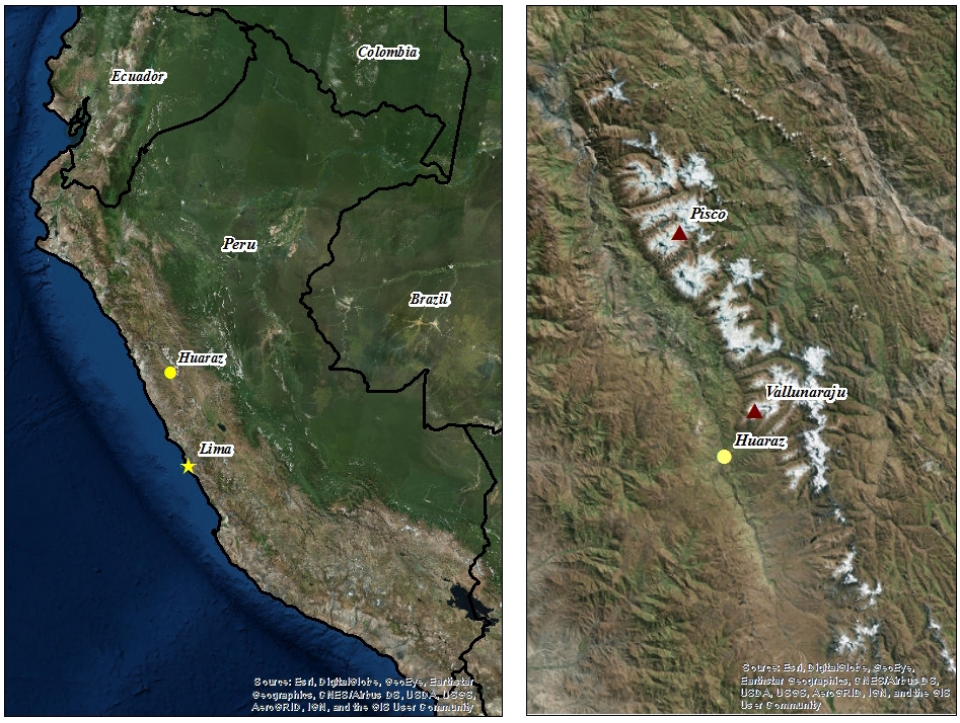

Figure 2: Maps of Peru (left) and the Cordillera Blanca with mountain field sites (right).

two locations within the Cordillera Blanca, Peru: Vallunaraju and Pisco (Figure 2). The duration period, solar energy per day, concentration of LAPs in the snowpack, and dry deposition come from raw data and are used to produce calculated values from the remaining variables within the model (Table 7).

The majority of hydrological models used in glacier-fed watersheds assume a snow albedo of 0.75, which neglects the impact that LAPs have on total glacier melt (Schmitt 2018). As such the aim of this model is to construct a model that may be incorporated into larger hydrological models in order to account for differences in albedo values due to LAPs both in the snowpack and on the surface.

7. Background

7.1 Glacier Dynamics

Glacier dynamics are largely influenced by surface energy balance and mass balance processes, both of which are governed by atmospheric and geographic variables. While the surface energy balance and mass balance of a glacier are not directly linked, surface energy balance processes influence mass balance through processes such as ablation, sublimation, and accumulation.

7.1.1 Surface Energy Budget Processes

The surface energy budget of a glacier is defined by the various heat and radiative fluxes that come in contact with the glacial surface. The surface energy balance is composed of shortwave and longwave radiation, subsurface heat flux, and turbulent heat flux. The net surface energy balance is a sum of all such components (Bamber and Payne 2004, Marshall 2012). Additionally, surface albedo heavily influences the surface energy balance of a

glacier, and is a critical component of the model presented in this study. Throughout the atmosphere, radiation is continuously absorbed and emitted at different levels. Flux at the surface is dependent on such processes, which mitigates glacier mass balance. While geothermal energy flux transmitted to the base of a glacier from the underlying earth has some impact on the total energy of the glacier, these values typically range between 0.04-0.06 W m^{-2} and are not nearly as impactful as the hundreds of watts per square meter produced by radiation fluxes at the atmospheric interface (Marshall 2012).

Snow and ice act both as energy storage units as well as shields against radiation (Slaymaker and Kelly 2007). Both mediums store latent heat and reflect most shortwave radiation and absorb and reemit most longwave radiation in the form of thermal energy (Slaymaker and Kelly 2007). Finally, snow and ice also act as insulators due to their porous structure, all of which influence the surface energy budget of snow and ice.

7.1.2 Short- and Longwave Radiation

Shortwave radiation is a key component of surface energy flux and balance. In most environments, shortwave radiation is the main cause of ablation (Marshall 2012). Incoming solar radiation is absorbed and scattered by suspended atmospheric particles such as dust and water vapor. Surficial incoming shortwave radiation is comprised of two main factors: direct and diffuse solar radiation. Reflection of direct light from surrounding terrain, largely influenced by the topography of an area, also influences isolation, but to a lesser extent. In addition to the direct solar bean, diffuse solar radiation reaches a location from all directions. This type of shortwave radiation arises from Rayleigh scattering off of atmospheric gases and Mie scattering off of aerosols, water droplets, and ice crystals. Diffuse radiation accounts for

the faint light that occurs when the sun is blocked out (Slaymaker and Kelly 2007, Marshall 2012) .

In addition to the influences of shortwave radiation, longwave radiation also controls energy flux at the glacial surface. Longwave radiation is comprised of infrared, thermal, and terrestrial radiation. Longwave flux to the surface comes from different heights, and therefore temperatures, in the atmosphere. This is because the air consists of different proportions of gases with different infrared emissivities. Water vapor and carbon dioxide are the main influencers of longwave radiation. However, longwave radiation is much more variable and difficult to predict without knowing the profiles of tropospheric water vapor, clouds, and temperature (Paterson 1994). Finally, net radiation is critical in the investigation of glacier surface energy budget because it is estimated that about 66% of energy available for ablation on glaciers comes from net radiation (Slaymaker and Kelly, 2007).

7.1.3 Glacier Accumulation and Ablation

Glacier mass balance is largely controlled by processes of accumulation and ablation. Such processes are the product of local climate as well as surface energy balance. While accumulation encompasses all processes that add material to a glacier, precipitation and deposition of atmospheric pollutants are those factors most influenced by climate change and the most relevant to this study. The accumulation of glacial ice usually takes place from snowfall, which is then transformed into ice through densification or consolidation. In dry conditions, grain packing, sintering (rounding), reduction of porosity and permeability, and recrystallization take place to transform snow to ice. Under dry conditions, this process can take up to 100 years. However, in wet conditions, the transformation of snow to ice occurs much more rapidly, because meltwater for surficial snowmelt can percolate into the snow and

refreeze further down. This reduces porosity and snow grain size thus accelerating the transformation process (Menzies 1995). While typically the amount of ice within a glacier increases overtime due to larger amounts of accumulation as compared to ablation over time, climate change has also caused an increase in the amount of ablation, leading to more ice loss than gain on many glaciers around the world.

Ablation defines all processes in which snow and ice are lost from the glacier. In general, the main cause of ablation is melting of snow and/or ice which is followed by run-off. At altitudes greater than 3,000 masl, sublimation, the process in which the phase change of a substance is from solid directly to gas, also plays a key role in ablation (Paterson 1994). Sublimation requires higher amounts of energy in order to transform snow or ice directly to vapor as compared to the amount of energy required to melt snow or ice. Ablation is largely controlled by the heat budget of a glacier which is in turn influenced by short- and longwave radiation at the surface.

7.1.4 Glacier Mass Balance: Topics and Methods

Glacier mass balance plays an important role in the how glaciers function over various time scales. Mass balance, also referred to as mass budget, is a measure of the amount of accumulation versus ablation on a glacier in a given year and is controlled by both atmospheric and geographic variables. A positive mass balance indicates more accumulation than ablation within a year; the reverse is true for a negative mass balance. In the steady state, inputs to the glacier via accumulation are equal to losses from ablation. Mass balance is a function of various external geographic and atmospheric relationships which influence the distribution and thickness of snow cover as well as the distribution and thickness of glacial ice. Aside from long- and shortwave radiation as well as ablation and accumulation, as

explained in the previous sections, mass balance is also a function of air temperature, and inputs of impurities from the atmosphere (Paterson 1994, Menzies 1995). Additionally, geographic variables such as altitude, topographic slope, and seasonal distribution of surface melt water influence glacier mass balance. In these factors, the atmosphere also mediates glacier mass balance through the deposition of pollutants.

Net mass balance is an important measure when studying glaciers in the long-term, especially in regards to climate change (Menzies 1995). There are various methodologies in which mass balance can be measured. Glaciological methods are commonly used to measure ablation at the surface by way of in situ data (Kaser et al. 2003). Additionally, photogrammetric methods can be used to examine change in mass balance in addition to creating detailed maps of glaciers. Finally, hydrological methods may be used to evaluate the amount of water stored in the glaciers via stream gauge readings (Kaser et al. 2003). While there are many other ways to measure glacier mass balance, the methods described above are the most common in the literature, specifically for mass balance studies situated in the Cordillera Blanca.

7.1.5 Climate Change and Glaciers

Snow reflects about 80% of incoming radiation from the sun as compared to the oceans and soils, which typically absorb 80% or more of incoming solar radiation (Slaymaker and Kelly 2007). This means that the amount of Earth's surface covered by ice and snow is critically important for global energy balance.

Measuring mass balance has become even more important since to start of the century due to increasing interest and urgency to understand the impact of climate change on glaciers. In the Cordillera Blanca, glaciers are especially vulnerable to climate change

because these glaciers are often exposed to melting or near melting temperatures on a daily basis. Thus, studying mass balance in the region has become of increasing interest.

High rates of glacier recession in the Cordillera Blanca began in the middle of the 19th century (Kaser and Georges 1999, Georges 2004). At the end of the Little Ice Age (LIA), the glacier extent of the Cordillera Blanca was 850-900 km^2 and retreated about 1000 meters by the onset of the 20th century (Georges 2004, Mark and Seltzer 2005, Vuille et al. 2008b). Similar rates of retreat were also found for the 20th century (Vuille et al. 2008b)

This loss of glacial volume is attributed to increased temperatures in the region accompanied by an increase in humidity as well as changes in precipitation (Mark and Seltzer 2005, Vuille et al. 2008b). Precipitation was found to be an important driver of mass balance in the Cordillera Blanca (Vuille et al. 2008a). However, it is difficult to separate the impacts of temperature and precipitation in the tropical Andes due to strong covariance between the two variables. Vuille et al. (2008b) found significant negative correlations between glacier mass balance in the Cordillera Blanca and tropical Pacific sea-surface temperatures (SSTs). This confirms previous results, as noted in section 4.1, that cold, La Niña years typically produce a positive mass balance while warm, El Niño years consistently have a negative mass balance (Kaser et al. 2003, Vuille et al. 2008b).

In addition to a general negative trend in mass balance, Bradley et al. (2009) reported an average of ~45m rise in freezing level height over the past 30 years. This result was also found to be strongly associated with El Niño-Southern Oscillation (ENSO) and mean tropical Pacific SSTs (Vuille and Bradley 2000, Vuille et al. 2003, Bradley et al. 2009). The above studies focus on changes in mass balance as a function of long- and shortwave radiation as

well as accumulation and ablation. In addition to such processes, glacier mass balance is also influenced by atmospheric deposition of pollutants onto the surface.

7.2 Atmospheric Deposition

Deposition of LAPs on glaciers is controlled by geochemical processes in the atmosphere as well as emission rates. Atmospheric deposition is the transfer of pollutants in the atmosphere to aquatic and terrestrial ecosystems. As the amount of anthropogenic pollutants, specifically via heavy industry, has increased, atmospheric deposition has become an field of increasing interest in the environmental science community due to the impact that such pollutants have on ecosystem health. Atmospheric deposition may occur through both dry and wet deposition.

7.2.1 Dry Deposition

Dry deposition is effectively the transport of particles and gasses from the atmosphere to Earth's surfaces without the influence of precipitation (Seinfeld and Pandis 2006). Atmospheric turbulence, the chemical properties of the deposited entity, and surface characteristics govern the deposition of particles and gases. In this paper, particulate matter and dust are the main focus. Size, density, and shape influence deposition of particulates and dust. Particles are transported towards the Earth's surface via turbulent diffusion. For lager particles, this process is enhanced due to their possession of inertia within the gravitational system. Small particles are governed more heavily by the deposition mechanics that act on gases because small particles do not experience inertia (Seinfeld and Pandis 2006).

7.2.2 Wet Deposition

Particulate matter may also be deposited from the atmosphere to Earth's surface via various types of wet deposition. Wet deposition is simply the removal of materials from the

atmosphere by hydrometeors such as rain and snow. However there are several different methods in which wet deposition of particulate matter may occur. Precipitation scavenging, or the removal of material from the atmosphere by raining clouds may occur in via rainout or washout. Below-cloud scavenging by falling snow or rain is defined as rainout whereas washout encompasses any scavenging of particles within a cloud (Seinfeld and Pandis 2006). In the Cordillera Blanca, wet deposition is mostly governed by snow deposition.

7.2.3 Pollutant Types

The most prominent types of atmospheric pollutants include: particulate matter containing heavy metals, polycyclic aromatic hydrocarbons (PAH), furans, sulphates, furans, nitrates, dioxins, and dust (Amodio et al. 2014).

These differing pollutants have influenced the framing of the field of study of atmospheric deposition. In the literature, studies may be divided into categories based on the type of pollutant being investigated (Table 1).

Table 1: Major themes presented in the literature on atmospheric deposition categorized by pollutant type.

Pollutant of Interest	Themes in Lit	References
Particulate matter	Concentrations of settled particles	(Ruijrok et al. 1995)
	Temporal variability	(Guo et al. 2014)
	Size distribution of particles	(Cao et al. 2011)
	Deposition flux	(Fang et al. 2004)
	Ambient concentrations	(Fang et al. 2007)
	Deposition velocities	
Organics	Polycyclic aromatic hydrocarbons	(Vassura et al. 2011)
	Polychlorinated dibenzo-p-dioxins	(Bergknut et al. 2011)
	Dibenzofurans	(Guo et al. 2014)
	Polychlorinated biphenyls	(Wu et al. 2005)
	Urban areas	(Castro-Jiménez et al. 2012)
		(Teil et al. 2004)
Inorganics	Metals	(Sakata et al. 2008)
	Ions	(Soriano et al. 2012)
		(Odabasi et al. 2002)
		(Hůnová et al. 2014)
		(Anatolaki and Tsitouridou 2007)
Mercury	Natural sources	(Pirrone et al. 2001)
	Coal combustion	(Pirrone et al. 2010)
	Mining	(Pacyna et al. 2001)
Biomonitors	Mosses and lichens	(Calamari et al. 1991)
	Plant species	(Blasco et al. 2006)
		(Bargagli et al. 2002)

Aerosols are colloids of solid particles liquid droplets suspended in the atmosphere. Human activities account for about 10-20% of all aerosols in today's atmosphere. Atmospheric deposition of aerosols can occur through three different processes: wet, dry (sedimentation), or occult deposition. Wet deposition may occur as rain washout or within a cloud when in-cloud scavenging or rainout takes place. Additionally, nucleation of droplets around particles may also occur. However, below a cloud, droplets and particles collide to form aerosols which are then deposited. Dry deposition processes, also referred to as sedimentation, do not involve precipitation. Finally, occult deposition processes involve fog, mist, or clouds (Amodio et al. 2014).

Most particulate matter deposited in both aquatic and terrestrial ecosystems occurs through dry deposition (Amodio et al. 2014).

In addition to the process in which pollutants are deposited, residence time also acts as an important factor in the process of atmospheric deposition. Most aerosols reside in the troposphere, from 0-15 kilometers above Earth's surface. The average residence time across all variations of aerosols in the troposphere is about five days. However, if aerosols reach the stratosphere (15-50 kilometers above Earth's surface), residence time increases significantly due to poor mixing of this atmospheric layer. Mean residence time, defined as the mass of particles over the inputs or losses from the atmosphere (flux), influences the level of impact that particles have on the atmosphere. Particles with longer residence times tend to be more harmful to the atmosphere because they are able to absorb more radiation over time and thus heat the atmosphere for longer.

Particles often times depart from their suspended state in the atmosphere and settle onto a surface on Earth. In such cases, the settling rate of particles becomes important because such rates influence the scale of impact that aerosols may have while still in suspension. Additionally, settling rates may give insight into the various sizes of suspended particles within a given area. Stokes' Law describes the rate of settling of particles in a given solution and is an important concept in atmospheric deposition. The rate of settling, according to Stoke's Law, is a function of the diameter of particles, the amount of particles added to the solution, viscosity of the solution, density of the solution, interactions between particles, shape of particles, density of particles, gravity, and velocity (Menzies 1995).

7.3 Light Absorbing Particles and Black Carbon

7.3.1 LAPs and Definitions of Black Carbon

Black carbon (BC) is a widely used term throughout the literature on atmospheric deposition. However, BC is loosely defined, with many studies using the same term with differing definitions as well as studies using different terms that assume the same definition. This makes it difficult to compare studies within the field. Additionally, there is little agreement on terminology that incorporates all aspects of the specific properties and measurement methods (Petzold et al. 2013).

Historically, there have been eight main terms used to discuss black carbon: organic carbon (OC), elemental carbon (EC), total carbon (TC), carbonate carbon (CC), black carbon (BC), primary carbon, secondary carbon, and soot (Table 2). Such definitions lack clear distinctions between terms and as such, studies within the literature do not adhere to the definitions presented in Table 2. Most commonly, elemental carbon, black carbon, and soot are used incorrectly as interchangeable terms.

As the research field regarding black carbon has gained attention, terminology has evolved to become more closely linked to various methodologies used within the field (Table 3). However, much like the historical terms before it, current terminology regarding black carbon also lacks clarity and exact detail to separate individual terms and avoid misuse (Petzold et al. 2013). Due to the persistent inconsistencies in the use of terminology within the field, Petzold et al. (2013) has presented a set of five terms to guide the reporting of black carbon-like substances in future studies (Table 3). Building from such terms, Petzold et al. (2013) has also presented a guide of recommended ways to report measurements based on commonly used techniques in the literature (Table 3).

Table 2: Fractions of carbonaceous aerosols sorted by historic definitions and associated methods.

Term	Definition	References
Organic Carbon (OC)	Any of the vast number of compounds where carbon is chemically combined with hydrogen and other elements such as O, S, N, P, Cl etc.	Petzold et al., 2013 Shaha and Rau, 1990
Elemental Carbon (EC)	A form of carbon that is essentially pure carbon rather than being chemically combined with hydrogen and/or oxygen. It can exist either in an amorphous or crystalline structure.	Petzold et al., 2013 Shaha and Rau, 1990
Total Carbon (TC)	Total particulate carbonaceous material; it is commonly assumed that TC= OC+EC and often neglects inorganic carbon	Novakov, 1984 Petzold et al., 2013 Shaha and Rau, 1990
Carbonate Carbon (CC)	Otherwise known as inorganic carbon (IC). Consisting of inorganic carbonate salts	Petzold et al., 2013 Shaha and Rau, 1990
Black Carbon (BC)	Combustion-produced black particulate carbon having a graphite-like microstructure or an "impure form of the element [carbon] produced by the incomplete combustion of fossil fuels and biomass. It contains over 60% carbon [by mass] with the major accessory elements hydrogen, oxygen, nitrogen, and sulfur."	Goldberg, 1985 Novakov, 1984 Petzold et al., 2013
Primary Carbon	Particulate carbon produced in sources, rather than in the atmosphere, being the sum of primary organic species and black carbon.	Novakov, 1984 Petzold et al., 2013
Secondary Carbon	Organic particulate carbon formed by atmospheric reactions from gaseous precursors. In current literature this fraction is referred to as secondary organic aerosol (SOA).	Novakov, 1984 Petzold et al., 2013
Soot	Synonymous with primary carbon derived from combustion or a common name for elemental carbon.	Novakov, 1984 Petzold et al., 2013 Shaha and Rau, 1990

Table 3: Recommended terminology regarding carbon by Petzold et al. 2013

Term	Definition
Total Carbon (TC)	Mass used to describe the mass of all carbonaceous matter in airborne particles
Black Carbon (BC)	Qualitative description when referring to light-absorbing carbonaceous substances in atmospheric aerosol; the term requires clarifications of the underlying determination for quantitative use
Equivalent Black Carbon (EBC)	Should be used instead of black carbon for data derived from optical absorptions methods, together with a suitable MAC for the conversion of light absorption coefficient into mass concentration
Refractory Black Carbon (rBC)	Should be used instead of black carbon for measurements derived from incandescence methods
Soot	Useful qualitative description when referring to carbonaceous particles formed from incomplete combustion.

Under the suggested reporting scheme from Petzold et al. (2013)**,** this study uses filter-based light-absorption techniques however, due to the amount of ambiguity within the

literature, we use the term light absorbing particles (LAP) when referring to the substance in question (Table 3).

For the purposes of this study, a light absorbing method was used and eBC (effective black carbon) is the reported term. However, pure BC acts as a blackbody, or a 100% absorptive surface. However, it is important to note that this does not mean that the object is black in color. Different surfaces may act as black bodies within various parts of the light spectrum. For example, snow can absorb all incident infra-red radiation, making it a blackbody in the infra-red part of the spectrum (Paterson 1994). However, in this study, we used methods concerning visible light, so while BC acts as a blackbody we are more concerned with albedo when considering the snowpack.

7.4.2 LAPs and Albedo

Albedo is a measure of the proportion of incident light that is reflected by a surface. This is calculated from short-wave radiation measurements. Specific surfaces have typical albedo ranges (Table 4) (Paterson 1994).

Table 4: Albedos of various snow and ice surfaces shown as percentages (Paterson 1994).

Surface	Range	Mean
Dry snow	80-97	84
Melting snow	66-88	74
Firn	43-69	53
Clean ice	34-51	40
Slightly dirty ice	26-33	29
Dirty ice	15-25	21
Debris-covered ice	10-15	12

The Snow, Ice and Aerosol Radiative (SNICAR) model is a multilayer model that produces a broadband snow albedo value by utilizing a two-stream radiative transfer scheme based on Toon et al. (1989) and Wiscombe and Warren (1980). A two-stream radiative transfer scheme divides the radiation field into the downward and upward fluxes of diffuse

radiation, meaning that radiation is scattered at least once, and the direct solar beam (Meador and Weaver 1980) (Amodio et al. 2014). The model considers incident radiation (diffuse or direct), solar zenith angle, surface spectral distribution, snow grain effective radius, snowpack thickness and density, and the albedo of the underlying ground as the principal variables. Back carbon concentrations (uncoated and sulfate-coated), dust concentrations broken down by size class, volcanic ash concentration, and an experimental particle concentration may also be used in the model in order to simulate the impact of impurities on snow albedo.

An output analysis of the SNICAR model found that snow grain size is heavily weighted in its influence of the model albedo output. Within the SNICAR model, snow grains are assumed to be spherical. This is similar to the methodology used in Wiscombe and Warren (1980) in which snow grain size acts as a proxy for snowpack age because grain size tends to increase as snow ages (LaChapelle 1969). In the SNICAR model, snow grain size also appears to act as a proxy for snowpack density.

7.4.3 Studies of LAPs on Snow and Ice

As demonstrated above, studies may define black carbon in different ways and approach their investigation of black carbon through various avenues. In the literature relating to the intersection between black carbon and snowpack or glaciers, many studies take a spatial or temporal approach. Ming et al examines the spatial distribution of soot in snow on glaciers in western China. While the authors use the term BC throughout the paper, they are referring to soot, or a product produced through the incomplete combustion of biofuel, fossil fuel, or biomass (Ming et al. 2009, Petzold et al. 2013). While many other studies throughout the literature also take a spatial approach to studying BC, Ming et al. (2009) use a

light absorption analysis method via a filtering technique, which tends to be a less chosen method.

Babu et al. (2011) also use a light absorption technique, however their study uses an aethalometer that measures suspended aerosol particles above glaciers. This study aims to investigate seasonal and temporal variations as well as apportion the source of suspended BC aerosols rather than take direct measurements of BC in the snowpack. While this technique does not provide in situ measurements of BC in the snowpack, it is able to produce abundant amounts of data.

While light absorption techniques are effective, refractory analysis methods are chosen to analyze measurements of thermal radiation more often. Specifically in regards to in situ measurements of BC on glaciers or in the snowpack, SP2 is the most common instrument used in refractory analysis of BC. Ginot et al. (2014), Kaspari et al. (2014), and Thomas et al. (2017) use SP2 to analyze snow samples from various glaciers around the world. Ginot et al. (2014) and Kaspari et al. (2014) investigate BC on glaciers in in the Khumbu region of Nepal, specifically on or near Mera Peak. Thomas et al. (2017) also use SP2 to quantify BC deposition on the Greenland ice sheet. SP2 tends to provide more accurate values of BC than light absorption techniques, and thus is commonly found in the literature, however it is also a more expensive technique.

Black carbon has been applied to a number of studies which examine various ecosystems. In this study, we examine the impacts of BC on glacier albedo in the Cordillera Blanca. Similar studies have been conducted throughout the Himalaya and in Greenland,

however the American Climber Science Program (ACSP) is one of the few groups that has investigated this field in South America, and more specifically in Peru.

8. System Behavior

8.1 Conceptual Model

The model was constructed on the basis of a basic snow energy budget (Figure 1). Incoming solar energy is partitioned into energy that enters into the snow system and energy that is reflected immediately at the surface. The energy that enters into the snow system is partitioned further into energy that is absorbed on the surface by LAPs, or the first wave of surface energy absorption, and energy that passes the surface and enters into the snowpack. Within the snowpack, a portion of the energy, between 60 and 63% of the total incoming solar energy, is reflected back towards the surface and out of the snowpack. This energy has a second opportunity to be absorbed by LAPs on the surface as they come into contact with these particles from below. The remaining energy in the snowpack is absorbed by LAPs and snow grains within the snowpack. All of the points of energy absorption, including the first and second wave of surface energy absorption and energy absorbed within the snowpack, contribute to snowmelt, which is assumed to washout at the bottom of the snowpack.

In the process of snowmelt, the model assumes that not washout of LAPs occurs. In other words, all LAPs contained within amount of snowmelt accumulate at the surface (Lazarcik et al. 2017). Additionally, in the operationalization of the model, LAPs on the surface are condensed into an area per square meter that is completely covered by LAPs and thus 100% absorptive (Figure 3).

The model uses the SNICAR albedo reduction value explained above is used in order to calculate the amount of energy that is absorbed within the snowpack (Equation 2). The SNICAR model produces a broadband snow albedo value for that of snow with no impurities and those with impurities (Figure concept snow energy model b). The difference in the albedo value between the pure and impure samples represents the fraction of the incoming solar radiation that is absorbed by the LAPs that would otherwise not be absorbed into the system. In this calculation, the 15% of total incoming energy reflected immediately at the surface is accounted for because the SNICAR output is a single broadband albedo value. Thus, in this model, and because the 15% immediate reflection at the surface is embedded in this SNCIAR calculation, the immediate reflection of energy at the surface is accounted for

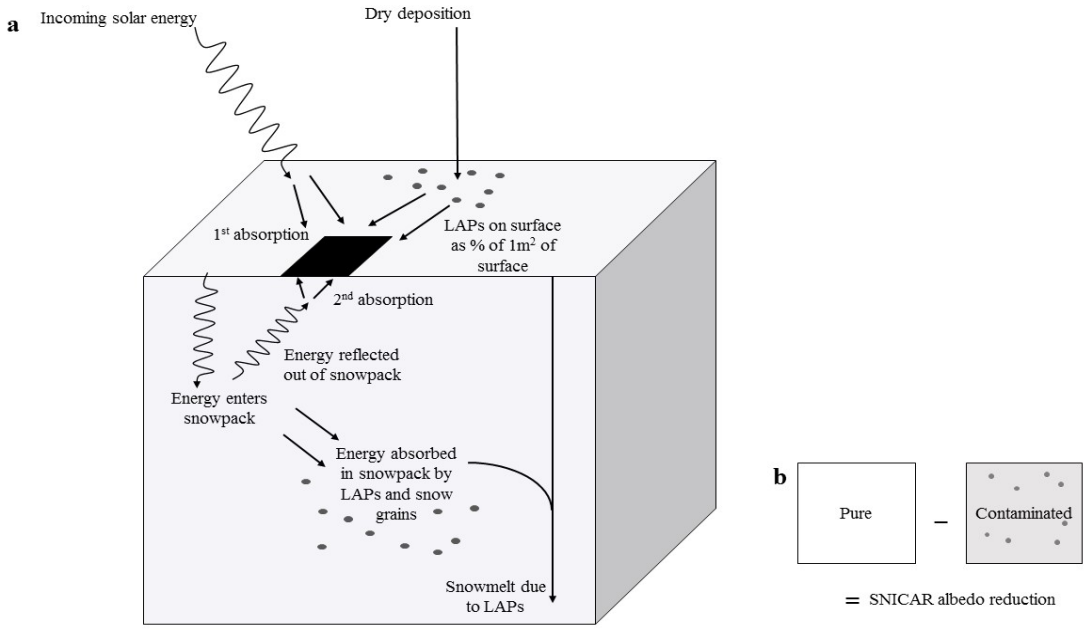

Figure 3: (a) conceptual model of the processes and their function within the model and (b) conceptual model of the SNICAR albedo reduction.

through SNICAR.

8.2 Model Refinement

During model construction, the product was restructured multiple times. At the onset, ranges for the inputs of the model were determined based on pervious literature and accessible datasets. For each value within the range, a scenario of the model was run. The output values produced by these were then analyzed in order to identify if a) the output values were within a reasonable range for each output variable, b) determine whether the functions and relationships within the model were reasonable, and c) identify areas in which details could be added. Based on the output analysis, the assumptions of the model were refined or redefined. The newly established assumptions influenced the revision of model equations based on the assumed relationships between variables. New relationships and equations oftentimes led to a new determined range of inputs or the model was rerun with the same input values.

Table 5: Input variables used in the model with their symbology, units, input ranges used to identify model behavior, and the sources of those ranges.

Variable	Symbol	Units	Input Range	Source
eBC concentration in snowpack	eBC_{sub}	ng g^{-1}	5-300	(Schmitt 2018)
Dry deposition	eBC_{dry}	ng m^{-2}	100-100000	(Schmitt 2018)
Day (duration)	d	Days	5-100	(Schmitt 2018)
Solar energy per day	E_e	J m^{-2} d^{-1}	10,000,000-20,000,000	(Schmitt 2018)
Degree-day	DD	Number of days with positive temperatures	0-4	(Schmitt 2018)
Degree-day factor	DDF	Mm d^{-1} $°C^{-1}$	2-8	(Schmitt 2018)
Substrate density	ρ	g cm^{-3}	0.3-0.9	(Schmitt 2018)

Table 6: Input values for in-snow eBC concentration and daily dry deposition for each simulated space.

Space	In-snow eBC concentration (ngg^{-1})	Daily dry deposition (ngm^{-2})	Source
Pisco	10	10,000	(Schmitt 2018)
Vallunaraju	30	40,000	(Schmitt 2018)
Clean Standard	0	0	

8.3 Model Variables

Table 7: Variables used in the model with symbology, units, and sources (equations or literature).

Variable	Symbol	Units	Source
Day	d	day	Determined by the number of days between weather events
Solar energy per day	E_e	J m^{-2} d^{-1}	(Rodriguez, 2017)
eBC concentration in snowpack	eBC_{sub}	ng g^{-1}	Filtered LAP samples taken from field locations analyzed for eBC concentration using LAHM
Amount of energy that interacts with clean snow within $1m^2$	E_{clean}	J m^{-2} d^{-1}	Equation 1
SNICAR albedo reduction	$\Delta\alpha$	Faction of total incoming energy that is reflected out of system	Calculation using input values derived from the SNICAR model and polynomial fit equation. Equation 3
Amount of energy absorbed within the snowpack per day	E_{sub}	J m^{-2} d^{-1}	Equation 2
Amount of energy absorbed on snow surface by eBC per day	E_{surf}	J m^{-2} d^{-1}	Equation 6
Snow mass loss due to eBC	m_{eBC}	kg m^{-2}	Equation 14
Snowmelt due to eBC	M_{eBC}	mm	Equation 15
Snow mass loss due to temperature	m_t	kg m^{-2}	Equation 18
Snowmelt due to temperature	M_t	mm	Equation 17
Snow mass loss due to eBC and temperature	m_{eBCt}	kg m^{-2} d^{-1}	Equations 19a and 19b
Snowmelt due to eBC and temperature	M_{eBCt}	mm	Equation 20
Cumulative snowmelt due to eBC and temperature	M_{sum}	mm	Equation 21
Amount of eBC to add to next day's surface value	eBC_{day}	ng m^{-2}	Equation 11
Mass of eBC on surface	eBC_m	g	Equation 10
eBC shaded area per meter squared snow	μ_{eBC}	m^2 m^{-2}	Equation 7
Percent of area covered by eBC within $1m^2$	$\%a_{eBC}$	fraction	Equation 8
Mass Absorption Cross Section	MAC	Meters squared per gram of eBC m^2 g^{-1}	Designated value for different LAP substances

Summed total amount eBC on snow surface	eBC_{total}	ng m^{-2}	Equations 12a and 12b
Dry deposition	eBC_{dry}	ng m^{-2}	Values based on literature of dry deposition based on geographic location
Albedo	α	Fraction: daily solar energy reflected at the surface over total daily solar energy	Equation 9
Degree day	DD	Number of days with temperatures over freezing per unit time	Equation 16
Degree day factor	DDF	mm d^{-1} $^{o}C^{-1}$	Input (Hock 2003), (Schmitt 2018)
Snow density	ρ	g cm^{-3}	(Schmitt 2018)
Additional energy absorbed on surface by eBC	E_{add}	J m^{-2}	Equation 5
Simulated surface eBC values	eBC_{sim}	ng g^{-1}	Equation 13

8.4 Model Equations

(d-1) is used to indicate that values from the previous day are used in the equation.

The total incoming solar energy (E_e) is partitioned between of the amount of energy that is absorbed on the surface (E_{surf}), the amount of energy absorbed within the snowpack (E_{sub}), and the amount of energy that is reflected out of the system, which is represented through albedo (α).

The amount of energy that interacts with clean snow within the $1m^2$ on the surface, E_{clean} (J m^{-2}) is calculated as

$$E_{clean} = E_e \times (1 - \mu_{eBC(d-1)}) \quad (1)$$

where E_e is the amount of total daily incoming solar energy (J m^{-2} d^{-1}), and $\mu_{eBC(d-1)}$ is the area within 1 m^2 covered completely by eBC (m^2 m^{-2}) from the previous day.

This is used to calculate the amount of energy that is absorbed within the snowpack, E_{sub} (J m^{-2}) which is expressed as

$$E_{sub} = E_{clean} \times \Delta\alpha \quad (2)$$

where $\Delta\alpha$ is the albedo difference from pure and contaminated snow, each of which are calculated using the SNICAR model, and the difference in $\Delta\alpha$ is calculated as Equation 3. In the model, a polynomial fit between SNICAR albedo outputs and eBC_{sub} values (0- 300 ng g^{-1}) (Equation 4) was calculated in order to calculate $\Delta\alpha$, on the basis of using the eBC in the snow, eBC_{sub}, at each time step without having to outsource calculations to SNICAR.

$$\Delta\alpha = \alpha_{pure} - \alpha_{eBC} \quad (3)$$

where α_{pure} is SNICAR albedo output value for snow containing no eBC and α_{eBC} is the SNICAR albedo output value for snow contaminated with a given amount of eBC and the fit with the model is done using a polynomial fit in JMP version 13.0.

$$\Delta\alpha = 0.0102321 + 0.0001312 \times eBC_{sub} - (1.6619 \times 10^{-7}) \times (eBC_{sub} - 145.5)^2 + (1.2034 \times 10^{-9}) \times (eBC_{sub} - 145.5)^3 - (5.859 \times 10^{-12}) \times (eBC_{sub} - 145.5)^4 \quad (4)$$

where eBC_{sub} ranges from 10-300 ngg^{-1}.

Through reflection of energy within the snowpack, a second wave of energy absorption by LAPs on the surface takes place (Figure 3). This additional absorption (E_{add}) (J m^{-2}) is expressed as

$$E_{add} = 0.65 \times (E_e - E_{clean}) \quad (5)$$

where 0.65 represents the proportion of the total incoming solar energy that is reflected out of the snowpack and E_e is is the daily amount of incoming solar energy (J m^{-2} d^{-1}) and E_{clean} is given in Equation 1.

The amount of energy that is absorbed within $1m^2$ on the surface from the first wave of absorption from the initial incoming solar energy is expressed as

$$E_{surf} = \mu_{eBC(d-1)} \times E_e \quad (6)$$

where E_e is the amount of daily incoming solar energy (J m^{-2} d^{-1}) and $\mu_{eBC(d-1)}$ is the area within $1m^2$ that is 100% shaded by eBC from the previous day (m^2 m^{-2}) and is expressed as

$$\mu_{eBC} = eBC_m \times MAC \quad (7)$$

where eBC_m is the mass of eBC on the surface within $1m^2$ (g) and MAC is the mass absorption cross section which represents the area that 1 gram of substance would cover the surface completely (m^2 g^{-1}).

The area covered by eBC, μ_{eBC}, is then converted to the percentage of $1m^2$ that is covered by eBC ($\%a_{eBC}$):

$$\%a_{eBC} = \left(1 - \%a_{eBC(d-1)}\right) \times \left(\mu_{eBC} - \mu_{eBC(d-1)}\right) + \%a_{eBC(d-1)} \quad (8)$$

where $\%a_{eBC(d-1)}$ is the percentage of 1 m^2 that is covered by eBC from the previous day.

This percentage is then used to calculate the albedo of the system using the following equation

$$\alpha = \alpha_{SNICAR} \times \left(1 - \%a_{eBC(d-1)}\right) \quad (9)$$

where α_{SNICAR} is the albedo of clean snow, which is initially calculated using SNICAR.

The mass of LAPs on the surface, eBC_m (g), used in Equation 7, is expressed as

$$eBC_m = \left(\frac{eBC_{day}}{10^9}\right) + \left(\frac{eBC_{dry(d-1)} + eBC_{m(d-1)}}{10^9}\right) \quad (10)$$

where eBC_{day} is the amount of eBC that has accumulated in a given time step (ng m^{-2}) as a function of the concentration due to snowmelt (Equation 11), eBC_{dry} is the amount of eBC accumulation due to dry deposition, eBC_{dry} (ng m^{-2}), and 10^9 is used to convert nanograms to grams.

The amount of eBC that is contained within the amount of snow mass lost for a given time step (eBC_{day})(ngm^{-2}) is assumed to accumulate on the surface and is added to the eBC value for the next day and expressed as

$$eBC_{day} = m_{eBCt} \times 1000 \times eBC_{sub} \quad (11)$$

where m_{eBCt} is the snow mass loss due to LAPs and temperature (kg m^{-2}) (Equation 14), eBC_{sub} is the concentration of eBC in the snowpack (ng g^{-1}) and 1000 is a conversion factor to convert from kg m^{-2} and ng g^{-1} to ng m^{-2}.

The total amount of eBC on the surface for a given day (eBC_{total}) (ng m^{-2}), which is representative of the amount that would be on the surface at the end of the day, may be expressed linearly or as a non-linear process. The linear process is expressed as

$$eBC_{total} = eBC_{total\,(d-1)} + eBC_{day} + eBC_{dry} \quad (12a)$$

where $eBC_{total(d-1)}$ is the total amount of eBC on the surface from the previous day (ngm^{-2}). eBC_{day} is defined by Equation 11, and eBC_{dry} is an input value (Table 5, 6, 7). The non-linear process is expressed as

$$eBC_{total} = eBC_{total(d-1)} + eBC_{dry(d-1)} + \left(\frac{\left(E_{sub(d-1)}+\left(\mu_{eBC(d-1)}\times E_{e(d-1)}\right)+E_{add(d-1)}\right)}{336000}\right)\times eBC_{sub(d-1)}\times 1000 \quad (12b)$$

where $eBC_{total\ (d-1)}$ is the total amount of eBC on the surface from the previous day (ng m^{-2}) (Equation 12b), $eBC_{dry(d-1)}$ is the amount of dry deposition from the previous day (ng m^{-2}) (Table 7), $E_{sub(d-1)}$ is the amount energy absorbed in the snowpack the previous day (J m^{-2}) (Equation 2), $\mu_{eBC(d-1)}$ is the area within $1m^2$ covered completely by eBC from the previous day (m^2 m^{-2}) (Equation 7), $E_{e(d-1)}$ is the total amount of incoming solar energy from the previous day (J m^{-2} d^{-1}) (Table 7), $E_{add(d-1)}$ is the amount of additional energy absorbed on the surface by LAPs from the previous day (J m^{-2}) (Equation 5), 336000 is the number of joules required to transform 1 kg of snow to liquid, $eBC_{sub(d-1)}$ is the concentration of in-snow eBC from the previous day (ng g^{-1}) (Table 7), and 1000 is a conversion factor to convert from kg m^{-2} and ng g^{-1} to ng m^{-2}.

.

The total surface eBC and subsurface values for a given time step are used to simulate an estimated surface concentration of eBC (eBC_{sim}) (ng g^{-1}) using the following equation

$$eBC_{sim} = \frac{eBC_{sub}+eBC_{total}}{(\rho\times 20000)} \quad (13)$$

where eBC_{sub} is the concentration of in-snow eBC (ng g^{-1}) (Table model variables), eBC_{total} is the total amount of eBC on the surface (ng m^{-2}) (Equations 12a and 12b), ρ is the density of the snow (g cm^{-3}) (Table 7) and 20,000 is used to convert ng g^{-1} to grams because the sample is assumed to have a depth of 2 cm.

The snow mass loss due to LAPs (m_{eBC}) (kgm^{-2}) is expressed as

$$m_{eBC} = \frac{E_{sub}+E_{surf}+E_{add}}{336000} \quad (14)$$

where E_{sub} is the amount of energy absorbed in the snowpack (J m^{-2}) (Equation 2), E_{surf} is the amount of energy absorbed on the surface (J m^{-2}) (Equation 6), E_{add} is the amount of additional absorbed by LAPs on the surface (J m^{-2}) (Equation 5), and 336000 is the number of joules required to transform 1 kg of snow to liquid.

Snow mass loss due to LAPs is converted to snowmelt (mm) using the following equation

$$M_{eBC} = \frac{m_{eBC}}{\rho} \quad (15)$$

where m_{eBC} is the snow mass loss due to LAPs (kg m^{-2}) (Equations 19a and 19b) and ρ is the density of the snow (g cm^{-3}) (Table 7).

Degree-days are used to calculate snow mass loss (kg m^{-2}) and snowmelt (mm) due to temperature within the model. A degree-day (DD) is a unit used to demonstrate the number of days, within a given time period, in which the average daily temperature is above freezing. In this model, degree-days are calculated separately (Equation 16) and then used as an input in the larger model. A degree-day factor (DDF) (mm d^{-1} $°C^{-1}$), also known as the melt

coefficient, is used in conjunction with the DD to calculate the snowmelt due to temperature (M_t) (mm). DD is expressed as

$$DD = \frac{(\sum_{i=1}^{24} T^+)}{24} \tag{16}$$

Where T^+ represents temperatures above 0°C, within a 24 hour period. Positive degree-hours are summed and then divided by 24 in order to convert from degree-hours to degree-days.

Snow melt due to temperature (M_t) (mm) is expressed as

$$M_t = DD \times DDF \tag{17}$$

where DD is degree days (Equation 16) and DDF is the degree day factor (mm d^{-1} $°C^{-1}$) (Table 7).

Snow mass loss due to temperature (kgm^{-2}) is expressed as

$$m_t = \frac{\left(\frac{M_t}{10}\right) \times 10{,}000}{1000} \tag{18}$$

where the conversions used to convert M_t (mm) to m_t (kg m^{-2}) workout so that $M_t = m_t$.

The amount of snow mass loss due to both LAPs and temperature (kg m^{-2}) is also calculated and is expressed as

$$m_{eBCt} = \left(\frac{E_{sub} + E_{surf} + E_{add}}{33600}\right) + m_t \tag{19a}$$

where E_{sub} is the amount of energy absorbed in the snowpack (J m^{-2}) (Equation 2), E_{surf} is the amount of energy absorbed on the surface (J m^{-2}) (Equation 6), E_{add} is the amount of

additional energy absorbed by LAPs on the surface in the second wave of absorption (J m^{-2}) (Equation 5), and m_t is the snow mass loss due to temperature (kg m^{-2}) (Equation 18).

Beyond the first time step, or first day, this may be expressed as

$$m_{eBCt} = m_{eBC} + m_t \quad (19b)$$

where m_{eBC} is the snow mass loss due to LAPs (kg m^{-2}) (Equation 14) and m_t is the snow mass loss due to temperature (kg m^{-2}) (Equation 18).

Snow mass loss is then converted into a snowmelt depth (M_{eBCt}) (mm) using the following equation

$$M_{eBCt} = \frac{m_{eBCt}}{\rho} \quad (20)$$

where m_{eBCt} is the snow mass loss due to LAPs and temperature (kg m^{-2}) (Equations 19 a and 19 b) and ρ is the density of the snow (g cm^{-3}) (Table 7).

The model also calculates the cumulative snowmelt depth for each time step (M_{sum}) (mm) by adding the previous day's cumulative snowmelt ($M_{sum(d-1)}$) to the snowmelt depth for the current time step (M_{eBCt}) (Equation 21)

$$M_{sum} = M_{sum(d-1)} + M_{eBCt} \quad (21)$$

8.5 Results

8.5.1 Value Ranges and Trends

Output values for E_{clean}, $E_{sub,}$ and albedo were all negatively and exponentially related to increased eBC_{sub} input values and E_{surf}, m_{eBC}, M_{eBC}, m_{eBCt}, M_{eBCt}, eBC_{day}, $eBC_{sim,}$

$eBC_{m,}$ eBC_{total} were positively and exponentially related to increased eBC_{sub} input values (Tables 5 and 7). M_t and m_t experienced no change from changes in eBC_{sub} values.

E_{clean}, $E_{sub,}$ E_{surf}, m_{eBC}, M_{eBC}, m_{eBCt}, M_{eBCt}, m_t, and M_t responded with reasonable output values when eBC_{sub} was between 0 and 40 ng g^{-1} (Table 7). eBC_{sim} values fell within a reasonable output range (0 - 1,500,000 ng g^{-1}) with eBC_{sub} values ranging from 0 to 110 ng g^{-1}. However eBC_{total} only responded reasonably to eBC_{sub} input values between 0 and 80 ng g^{-1} in order to fall within a reasonable output range from 0 to $1.3x10^9$ ng m^{-2}. eBC_{day} and albedo outputs responded with a reasonable range of output values when eBC_{sub} input value limit was 20 ng g^{-1} and 10 ng g^{-1}, respectively.

In addition to eBC_{sub}, output values of eBC_{sim} and albedo were also dramatically impacted by the input values used for eBC_{dry}, DD, and DDF. eBC_{sim} output values were positively and exponentially related to $eBC_{dry,}$ DD, and DDF values while albedo had a exponentially negative relationship with increases in eBC_{dry} and DD values. eBC_{sim} and albedo outputs were only reasonable when eBC_{dry} input values fell between 0 and 50 ng m^{-2}. eBC_{dry} values of 100 ng m^{-2} produced eBC_{sim} values of 650 ng g^{-1} or greater. Albedo was reduced by 0.03 or more when eBC_{dry} values of 100 ng m^{-2} or greater were used.

DD values beyond 0.75 yielded albedo reductions greater than 0.02 and eBC_{sim} values greater than 450 ng g^{-1}. Albedo had a negative non-linear relationship with increased DDF values, however the relationship was not exponential like its relationships with eBC_{sub}, eBC_{dry}, and DD values. DDF values beyond 2 mm $d^{-1}°C^{-1}$ resulted in a simulated albedo reduction of 0.02 or greater. eBC_{sim} shared a positive non-linear relationship with increased DDF values, and like albedo, the relationship was not exponential. DDF values of 2 $d^{-1}°C^{-1}$

or greater resulted in eBC_{sim} values of 500 ng g^{-1} or greater. Simulations for DDF values less than 2 $d^{-1}°C^{-1}$ were not run.

E_e and M_{sum} shared a positive non-linear relationship in which increased E_e values resulted in higher values of M_{sum}. Additionally, this relationship was amplified over the course of the 90 day run in which the change in M_{sum} became larger between days starting around day 35 and becoming most amplified between days 70 and 90 (Figure 4). The maximum amount of cumulative snowmelt (1461.3 mm) occurred under 20,000,000 J m^{-2} d^{-1}

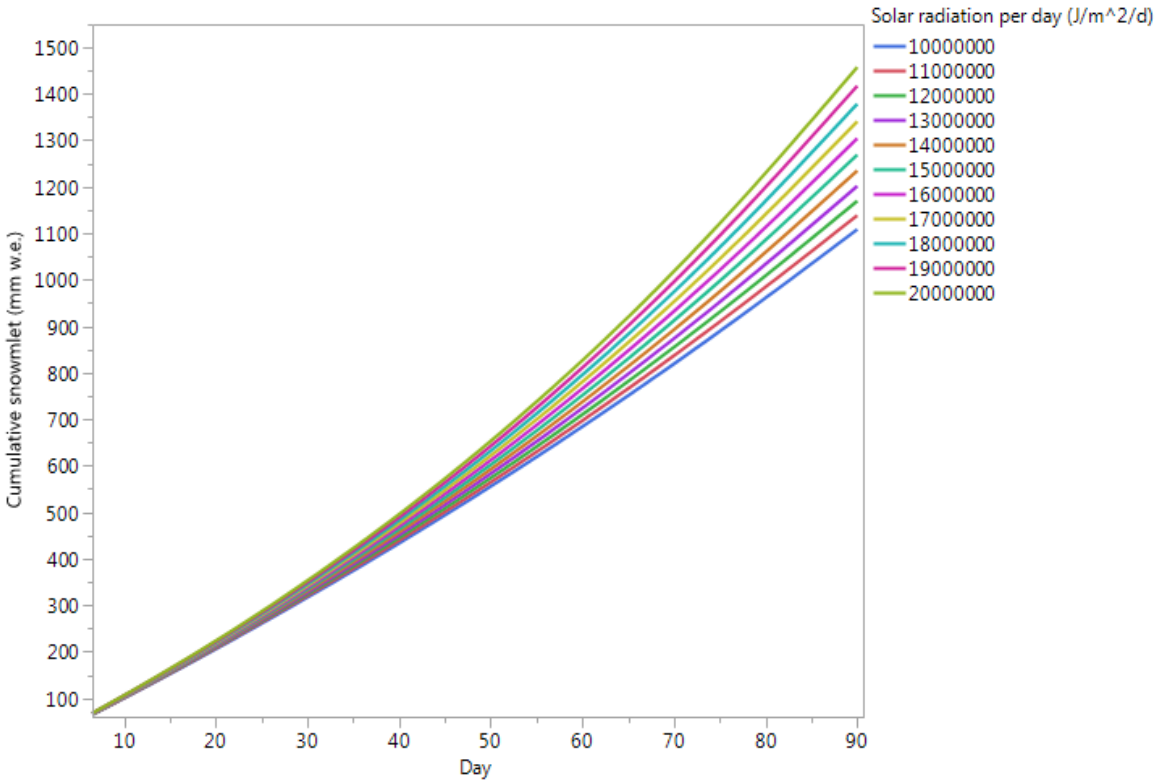

Figure 4: Cumulative snowmelt over the course of 90-day runs at each day for 1,000,000 E_e intervals between 10,000,000 and 20,000,000 J m^{-2} d^{-1}.

on day 90 whereas the simulation with 10,000,000 E_e resulted in 1109.7 mm snowmelt on day 90 (Figure 4).

M_{eBCt} also increased as eBC_{total} increased, but did so at a decreasing rate. Larger values of eBC_{sub} also yielded larger amounts of eBC_{total}. eBC_{day}, and eBC_{sim}. eBC_{sim} values equated to between 0.167 and 0.169% of eBC_{total} for each day within a run (Figure 5).

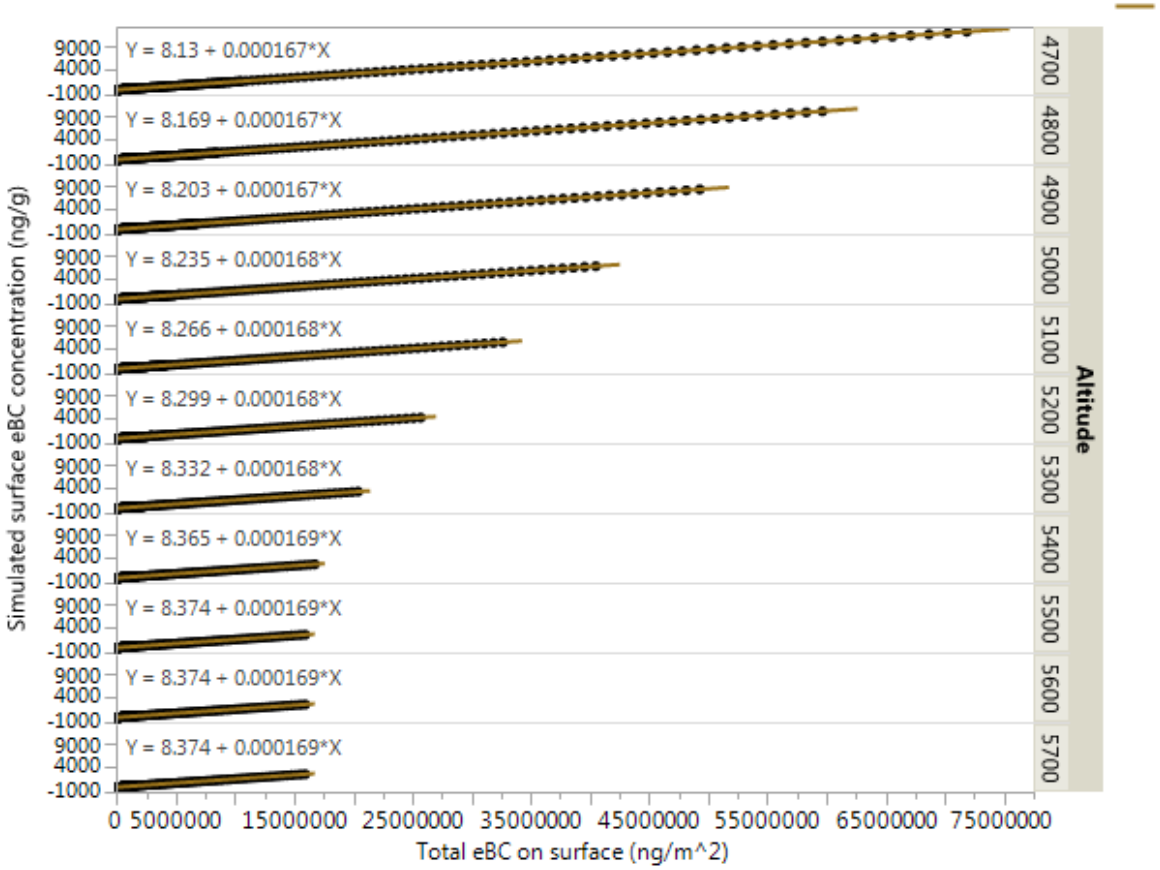

Figure 5: eBC_{sim} values compared against eBC_{total} values on an altitudinal gradient from 4700 to 5700 masl with an interval of 100 m.

A negative relationship between altitude and E_{surf} led to decreased values for M_{eBCt} and M_{eBC} as altitude increased (Figure 6 a and b). M_t also decreased as altitude increased but this was driven by a decrease in DD values as altitude increased (Figure 6a) (Table 8). As m_{eBCt} increased albedo was reduced with reductions as large as 0.3 (Figure 6c). There was more reduction in albedo at lower elevations, which was driven by up to 45 kg m^{-2} of snow

mass loss (Figure 6c). M_t and M_{eBC} together made up the value of M_{sum} at each elevation, which decreased exponentially as altitude increased, driven by a negative relationship between altitude and DD values (Table 8) (Figure 7). Thus, M_{eBC} increased by a factor of M_t, which decreased with altitude (Figure 7). Additionally, at 5500 masl and above, M_t went to 0 as there were calculated to be no degree-days (Figure 7).

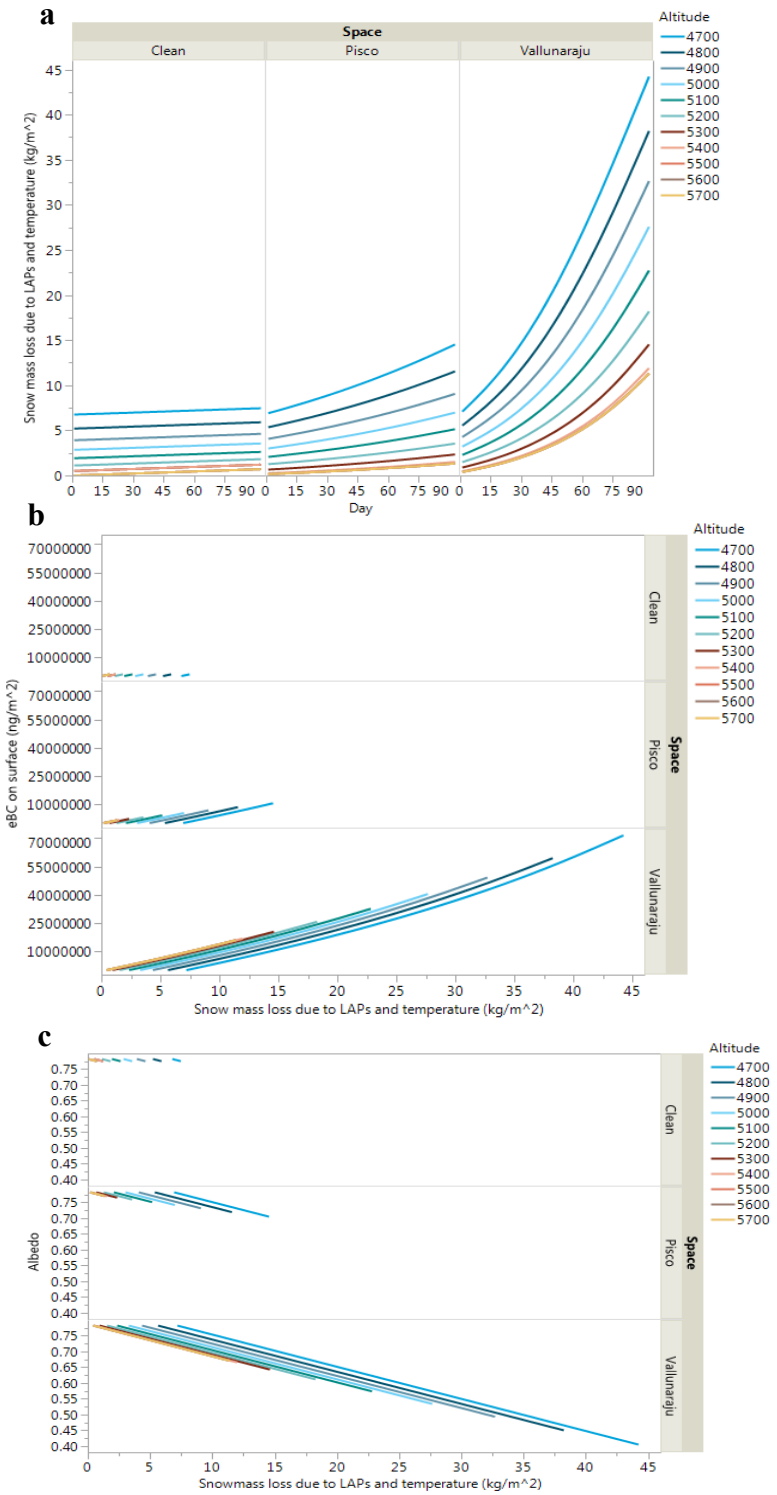

Figure 6: (a) snow mass loss due to LAPs and temperature over the course of 93 day runs, (b) total eBC on the surface per day by the snow mass lost due to LAPs and temperature, and (c) albedo by snow mass loss due to LAPs and temperature for all altitudes for the clean standard, Pisco, and Vallunaraju

Table 8: Calculated degree day values and their corresponding snowmelt values for each simulated altitude.

Altitude (masl)	Degree Day	Snowmelt due to temperature per day (mm)
4700	2.703	6.756
4800	2.08	5.12
4900	1.565	3.912
5000	1.139	2.847
5100	0.765	1.913
5200	0.443	1.107
5300	0.201	0.502
5400	0.036	0.09
5500	0	0
5600	0	0
5700	0	0

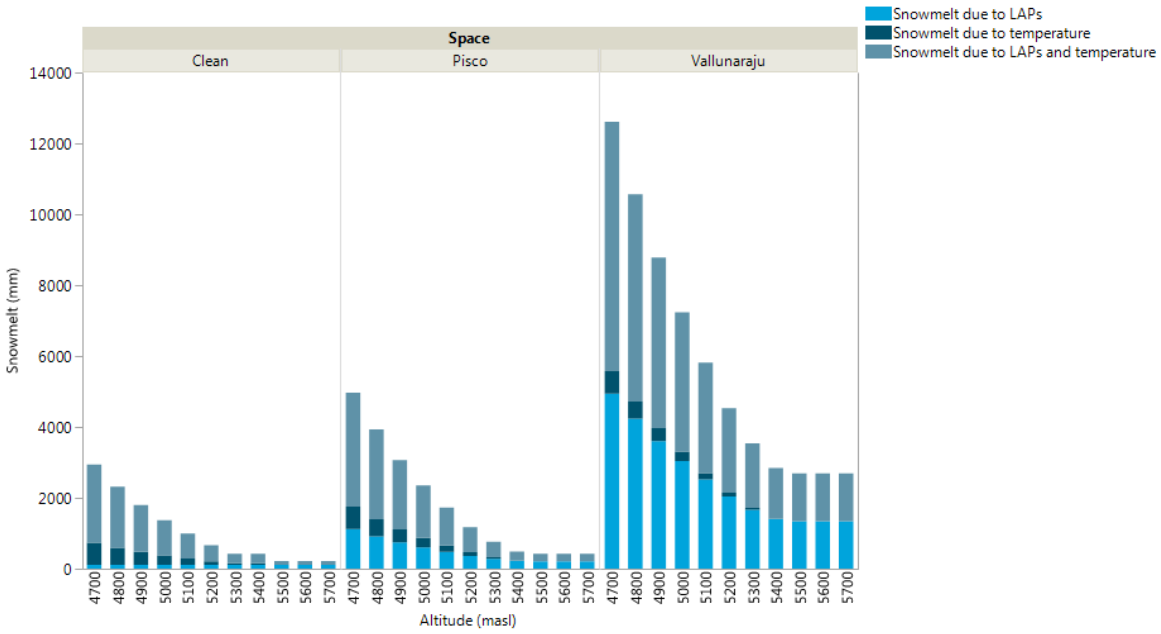

Figure 7: Total snowmelt (mm) for each altitude separated by space. Total snowmelt is displayed as proportion due to LAPs and proportion due to temperature.

8.5.3 eBC in Snow Variation

At 4700 masl, where M_t was highest, a concentration of 10 ng g^{-1} resulted in a 0.01 albedo reduction over the course of 16 days (Figure 8). At altitudes where M_t did not occur (Table 8), the same reduction in albedo took place over the course of 81 days (Figure 8). At 4700 masl, for simulations that used an eBC_{sub} input of 30 ng g^{-1}, an albedo reduction of 0.01 took place over the course of 10 days (Figure 8). However at 5500 masl and above, where there were no degree days (Table 8) and no snowmelt due to temperature occurred, an albedo of reduction of 0.01 took place over the course of 21 days (Figure 8).

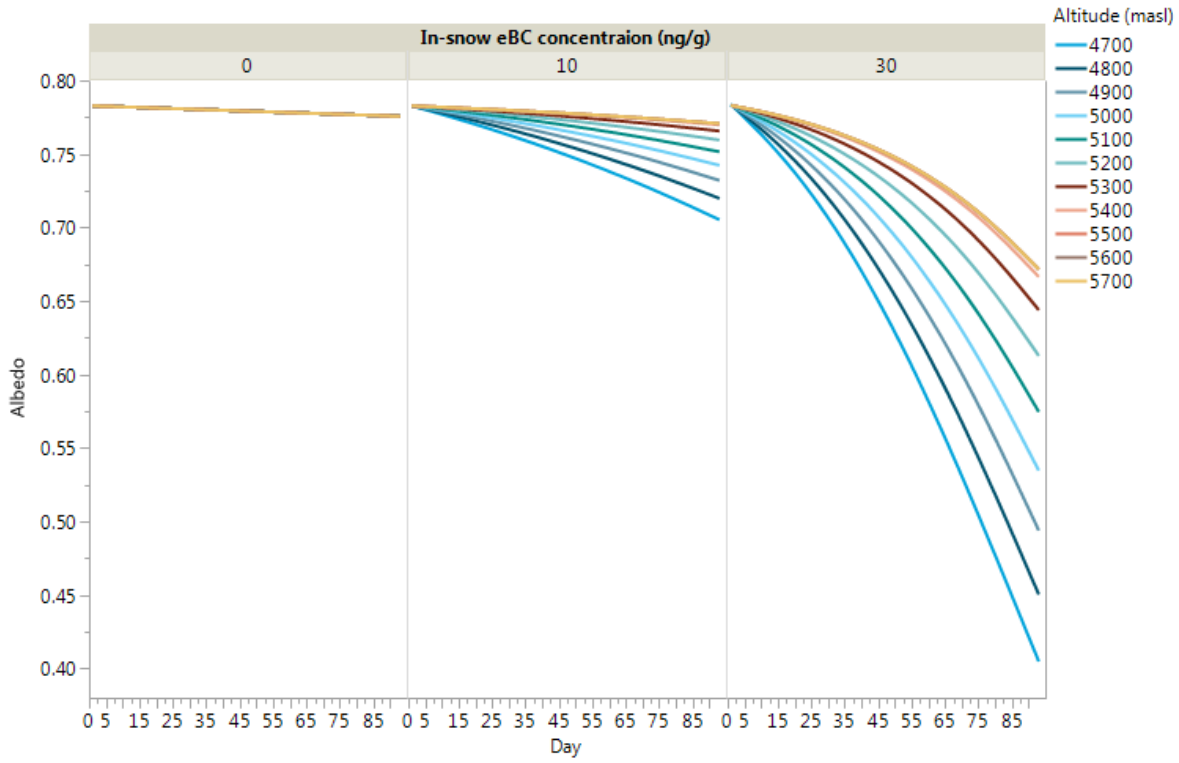

Figure 8: Albedo trends for simulations on an altitudinal gradient with a 100 m interval over the course of 90-day runs for simulations run with 0, 10, and 30 ng g^{-1}.

8.5.4 Run Duration Variation

The previously stated results are all based on 90-day simulation runs. While the duration itself did not push the model beyond its limits, longer simulation durations allowed for larger amounts of accumulation of eBC_{total} on the surface. This resulted in larger simulated albedo reductions and values of E_{sub}, E_{clean}, and E_{surf} that went beyond reasonable ranges of energy absorption. As run duration decreased, eBC_{total} accumulation was restricted thus a higher proportion of E_e entered into the snowpack and a was absorbed within the snowpack. Decreased run durations also resulted in a lower proportion of total incoming energy being absorbed on the surface, overall. For 45-day simulation runs, under conditions between 0 and 70 ng g^{-1} eBC_{sub}, E_{sub}, E_{clean}, and E_{surf} values all fell within their determined ranges of reasonable outputs. Finally, snowpack density, ranging from loosely packed snow to ice, affected M_{eBCt} and M_{eBC}. Both M_{eBCt} and M_{eBC} values decreased as snowpack density increased.

8.6 Discussion

The 40 ng g^{-1} upper limit of the eBC_{sub} input value for the majority of output variables in the model, including E_{clean}, $E_{sub,}$ E_{surf}, m_{eBC}, M_{eBC}, m_{eBCt}, M_{eBCt}, m_t, and M_t, is likely due to the 90-day duration of the runs and the assumption that no outwash of eBC takes place. The majority of LAPs are water-insoluable, which causes them to accumulate at the surface instead of being washed out with snowmelt. Because this model function in between snow accumulation events, eBC accumulates exponentially on the surface over the course of the run and allows for incredibly high values of eBC_{total} to exist on the surface (Equation 12b), which explains why shorter runs had a higher upper limit for the input value of eBC_{sub}.

Xu et al. (2012) found that over the course of a one-year experiment the concentration of black soot was enriched by at least an order of magnitude as compared to the original concentration in snow at the beginning of the year. Summer snow surface BC values were 13 times higher than winter values from January and February, with concentrations as high as 400 ng g^{-1} (Xu et al. 2012). Increased surface LAP values due to the accumulation of LAPs previous held within the snowpack before melt increase the amount of energy absorbed on the surface and further reduce broadband albedo. The magnitude of this positive feedback is largely dependent on the scavenging efficiency of LAPs and LAP particle size (Doherty et al. 2013, Schwarz et al. 2013). Other studies have also found that 10 ngg^{-1} of eBC yields a 0.01 reduction of albedo values. Xu et al. (2009) found that an increase of 10 ngg^{-1} of eBC on the surface yielded an albedo reduction between 0.01 and 0.04.

As LAPs accumulate on the surface, both through the process of snowmelt and dry deposition, LAPs are randomly distributed and are able to accumulate on top of one another. At low values of μ_{eBC}, this does not appear to pose a problem for calculating the area shaded by LAPs. However, as values approach 1, where the entire square meter is covered by LAPs, the function falls apart. This is because the models assumes a linear fit for this process when in reality it becomes exponential when values approach 1. Such assumptions then impact the calculation of energy that enters into the snowpack, energy absorbed within the snowpack, and albedo.

Dry deposition values used in model runs had a large impact on $eBC_{day,}$ eBC_{sim}, and eBC_{total} output values because of the operationalization of each of these variables within the model (Equations 11, 12a, 12b, and 13). Dry deposition is difficult to measure and little literature exists regarding dry deposition rates in the Cordillera Blanca. Values used in these

simulations are based on findings presented in Yasunari et al. (2013). The study estimated dry deposition values between 900 and 1300 μg m^{-2}, which converts to 900,000 to 1,300,000 ng m^{-2} (Yasunari et al. 2013). Dry deposition values this large overloaded the model and produced unreasonable albedo output values. However Yasunari et al. (2013) reported that dry deposition values within this range have the potential to reduce broadband albedo values anywhere from 5.5-8.4% depending on the age of the snow. As such, dry deposition values used in these simulations present a site of large uncertainty due to the uncertainty in deposition rates in the Cordillera Blanca.

Snowmelt values varied mainly due to in-snow eBC concentrations and temperature, and thus altitude. While it is likely that the assumption of LAPs accumulation on the surface used in the model is a main driver in the impact that in-snow eBC values have on snowmelt and albedo, temperature is presented as a constant value based on altitude within the model. Snowmelt values were lower and albedo values higher with increased altitude. In this model, this is driven by changes in temperature and thus the degree-day value used in the simulations at different altitudes. While temperature plays an important role in glacier ablation, specifically within the Cordillera Blanca, it is not the most prominent cause of ablation in the region (Vuille et al. 2008b).

Gurgiser et al. (2013) found that ablation rates were low above 5000 masl at Shallap glacier in the Cordillera Blacna, which may suggest that the model over estimates snowmelt due to temperature between 5000 and 5100 masl where a degree day value of 1.139 and 0.765 are used, respectively. At 5200 masl and above, degree day values used in the model are lower (≤0.443) however at 5000 and 5100 masl, DD values used in simulations may have been too high, causing the model to overestimate the amount of melt due to temperature. This

is assuming that the characteristics of ablation found by Gurgiser et al. (2013) at Shallap glacier are somewhat consistent across a larger area of the Cordillera Blanca. Gurgiser et al. (2013) also reported that the absorption of solar radiation had a large impact on the high melt rates that were present in the Shallap glacier ablation zone. This has implications for the model presented in this study because Gurgiser et al. (2013) did not account for absorption due LAPs in the glacial system. Because increases in surface concentrations yield higher rates of solar energy absorption, Gurgiser et al.'s (2013) study further indicates that melt rates are indirectly linked to eBC surface concentrations.

The equilibrium line altitude (ELA) and changes in precipitation on an attitudinal gradient play important roles in ablation in the Cordillera Blanca (Mark and Seltzer 2005, Vuille et al. 2008b). This model functions in between precipitation events and thus does not take into account for ablation mitigation caused by precipitation events. Vuille et al. (2008b) found a highly significant correlation ($p<0.01$) precipitation and glacier mass balance in the Cordillera Blanca. However, it is still unclear as to whether the large impacts of precipitation on mass balance were directly caused by accumulation or indirectly through increase in surface albedo and the amount of radiation that enters into the snowpack system (Vuille et al. 2008b).

Additionally, the model does not account for snow mass loss due to sublimation, which may impact snow mass loss estimates and thus surface eBC concentrations due to surface aggregation during the melt process (Xu et al. 2013 Doherty et al 2013). However, in the Cordillera Blanca, multiple studies have found that sublimation accounts for much less ablation as compared to snowmelt (Wagnon et al. 1999a, Wagnon et al. 1999b, Mark and

Seltzer 2005, Vuille et al. 2008b, Gurgiser et al. 2013) but sublimation is still accounts for a notable amount of total mass lost.

Vuille et al. (2008b) found that sublimation was limited in the Cordillera Blanca and more snow mass loss was due to melting. This was due to a negative correlation between near-surface vapor pressure and mass balance, caused by increased near-surface humidity. The reduced vapor pressure gradient between the glacier surface and the air above lowered latent heat flux which limited sublimation (Vuille et al 2008b). Available solar energy was used in the process of melting due to melting's 8.5 times more efficient use of energy as compared to sublimation, which caused more mass loss through melting (Vuille et al 2008b).

Mark and Seltzer **(2005)** found that sublimation counted for 20% of ablation within one hydrological year in the Cordillera Blanca. Wagnon et al (1999a) noted negative latent heat fluxes for the Zongo Glacier in the Cordillera Real, Bolivia. This led to ice mass loss at the surface via sublimation, with high rates of sublimation during the dry season, which is the same as the dry season in the Cordillera Blanca (Wagnon et al. 1999a). However, sublimation still only accounted for 202 mm of 1196 mm of total ablation, or about 17% over the entire hydrological year. This value is comparable to that reported by Mark and Seltzer (2005), suggesting that sublimation in the dry season in the Cordillera Blanca may fluctuate around 20% of the total ablation.

9. Simulations

9.1 Pisco Simulations

9.1.1 Methods

Simulated surface eBC concentration output values were compared with field samples from the col and summit of Pisco for the 2012 dry season in order to simulate real-world LAP accumulation on the glacial surface. The samples were collected by the American Climber Science Program in two sets from Pisco on June 15th and August 1st, 2012. Samples were taken from glacial surfaces along an altitudinal transect. At each sampling location snow was taken from the surface (1-3 cm in depth) and a subsurface (3-5 cm in depth) directly below the area where a surface sample was taken. Enough snow was collected for each sample to fill a 4-liter resealable bag.

After collection, samples were melted one at a time by placing each plastic bag in warm water (around 30ºC). Samples were subsequently filtered. Filtering took place immediately after melting in order to minimize adhesion of particles to the surface of the plastic bag. The resulting water from the snow was drawn up into a 60mL syringe and pumped slowly through a 0.7 micron Pallflex® Tissuquartz type 25mm quartz fiber filter which was attached to the syringe by a filter holder. A single filter was used for each melted snow sample. Water was filtered until the filter presented obvious discoloration. A maximum of 600 mL of water was filtered for each sample as to avoid overloading the filters with LAPs.

After the filtering process was complete, filters were dried in the sun and then placed into individual storage capsules and stored in a freezer. Filters were then analyzed for an eBC concentration using the protocol detailed in Appendix A.

45-day simulations were run for the col and the summit in order to simulate eBC concentration changes within the system between June 15th and August 1st, 2012. Multiple simulations were run at the col using a range of dry deposition values and a single simulation as the summit (Table 9). Additionally, simulations for the summit and the col used different input values based on the each space's physical characteristics including altitude, snowpack density, and eBC_{sub} values (Table 9).

Table 9: Input values used in the different simulations run for the Pisco col and summit.

Space	Run #	Days	E_e	eBC_{sub}	eBC_{dry}	ρ	DD	DDF	SNICAR α_{eBC}
Col									
	1	45	$1.62x10^7$	7.6	0	0.6	0.201	2.5	0.7798
	2	45	$1.62x10^7$	6	0	0.6	0.201	2.5	0.7804
	3	45	$1.62x10^7$	7.6	5200	0.6	0.201	2.5	0.7798
	4	45	$1.62x10^7$	7.6	2000	0.6	0.201	2.5	0.7798
Summit									
	1	45	$1.62x10^7$	6	5200	0.3	0	2.5	0.7804

9.1.2 Results

Simulation Col 3 used 6 ng g^{-1} eBC_{sub}, as compared to 7.6 ng g^{-1} eBC_{sub} used in all three of the other col simulations, and had the smallest change in the concentration of surface eBC of the group (Table 9, Figure 9 a and b). This mirrored the strong impacts that eBC_{sub} values had on model output variables described in section 8.5 and 8.6. Additionally, measured eBC_{sim} values at the col were larger than those at the summit on June 15th (day 1) however, the eBC_{sim} value of the summit surpassed that at the col between days 12 and 15 and eBC_{sim} values of 20 to 25 ng g^{-1} (Figure surf eBC day summit col b). At the end of the simulation, the eBC_{sim} values at the col were within ±22.1 ng g^{-1} of the measured eBC surface concentration of 35.8 ng g^{-1} (Figure 9 a and b). Finally, for over the course of the 45-day simulation, the model produced a albedo reductions between 0.001 and 0.0039 at col while the summit had an albedo reduction of 0.0022 (Figure 9 c).

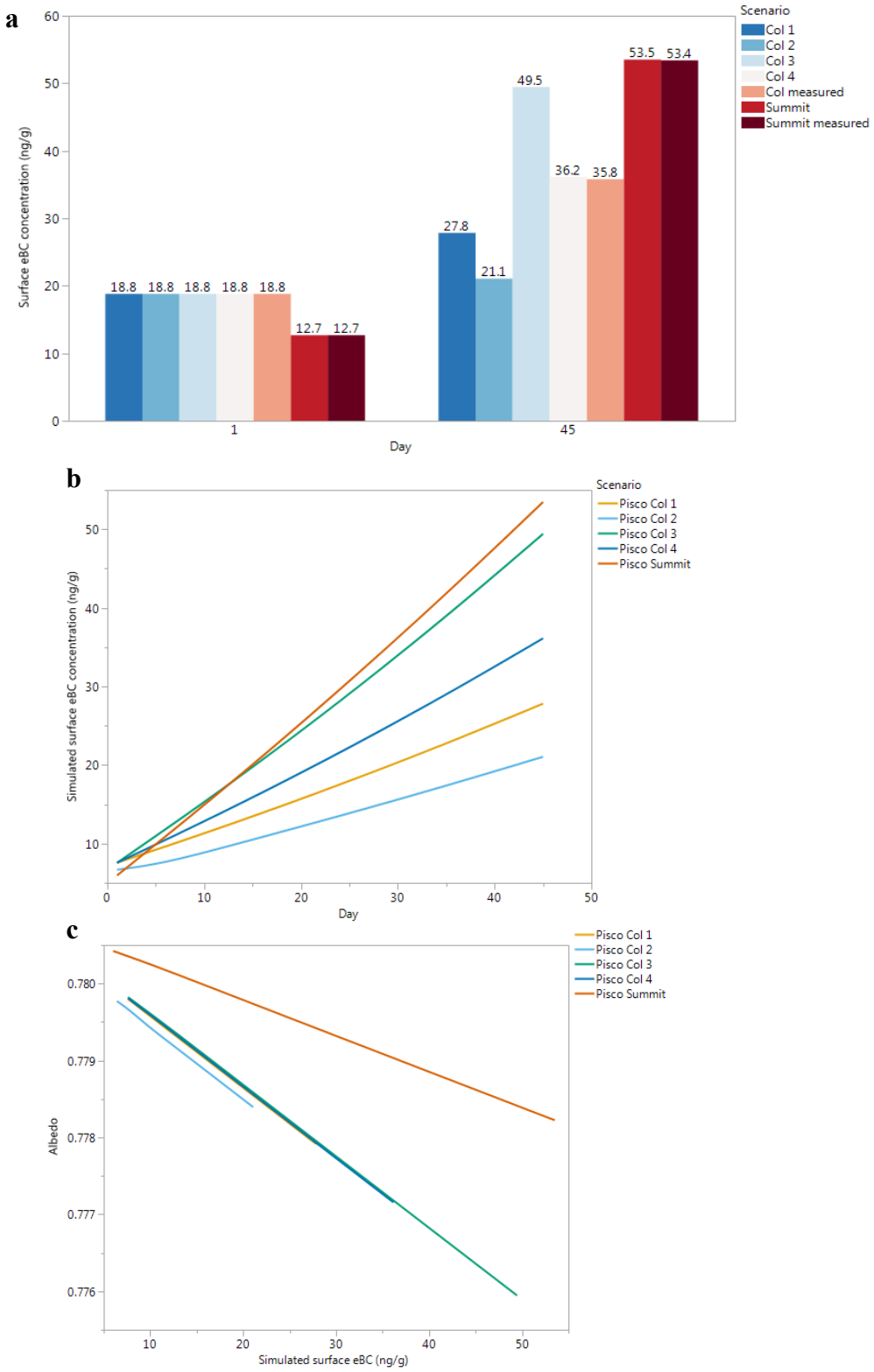

Figure 9: (a) Measured and simulated surface eBC concentrations at the onset of the run (day 1) and the end of the run (day 45) for the Pisco col and summit. (b) Daily simulated values of surface eBC concentration over the course of a 45 day run for the Pisco col and summit. (c) albedo change by the simulated surface eBC concentration.

experienced a more rapid decrease in the surface albedo as compared to the summit (Figure 9 c).

Over the entire 45-day run, more snowmelt occurred in all four simulations at the col compared to the 31.9 mm of snowmelt that occurred at the summit (Figure 10). Because the summit is situated at 5700 masl and the DD value is 0, no melt due to temperature occurred at the summit. At the col, melt by temperature increased daily values of M_{eBC} by 0.502 mm, or 22.6 mm over the course of the 45-day run. Snowmelt due to LAPs varied across all of the col simulations, with the Col 3 simulation resulting 23.6 mm M_{eBC}, the highest value of M_{eBC} of all four col simulations. The 31.9 mm of M_{eBC} at the summit, which also represented the total snowmelt at the summit, was the highest M_{eBC} value of all five simulations (Figure 10).

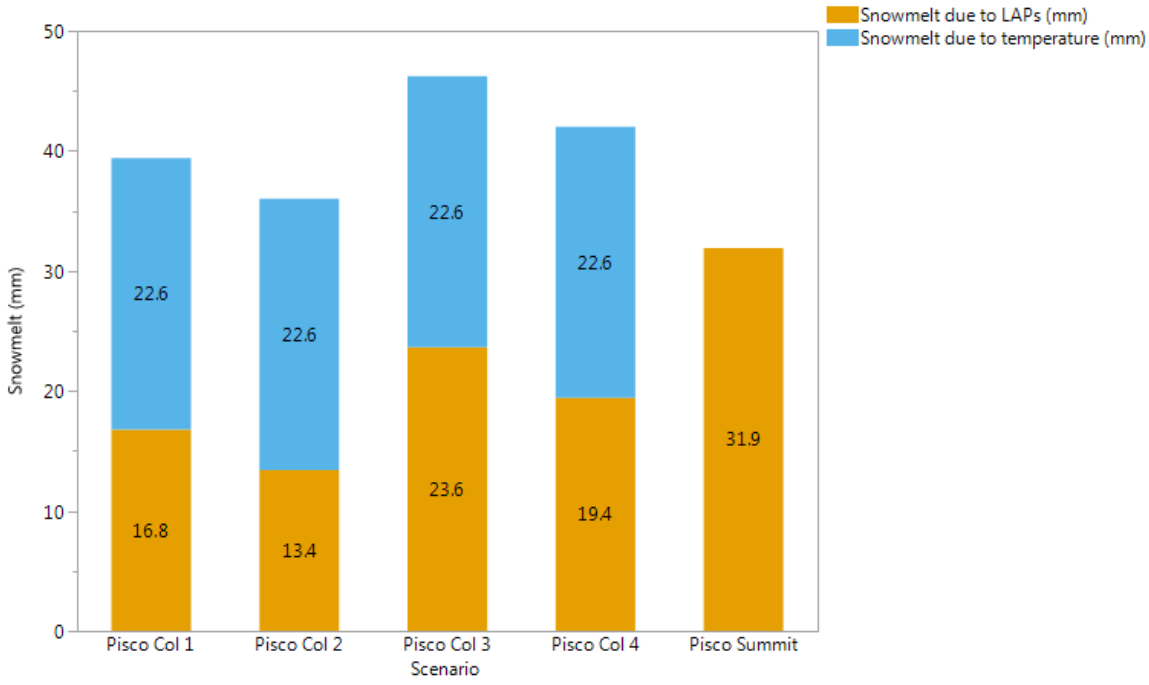

Figure 10: Total snowmelt for each Pisco simulation at the col and summit. Total melt is displayed as the proportion due to LAPs and the proportion due to temperature.

9.1.3 Discussion

The Col 4 run best simulated the accumulation of LAPs on the surface at the col. However, the Col 4 simulation used different input values for eBC_{dry} and eBC_{sub} from those of the summit simulation (Table 9). Hicks (1986) presented a model for estimating dry deposition rates in mountainous environments and suggested that deposition rates are likely higher on high-altitude slopes. However, the study does not present quantitative results to firmly suggest that dry deposition rates regularly increase with altitude (Hicks 1986). Additionally, local climatic patterns, specifically wind patterns, play a large role in dry deposition patterns. In regards to the Cordillera Blanca, weather systems that move into the Andes from the Amazon basin due to easterly winds might suggest that increased rates of wet deposition occur on the eastern slope of the range, but do not give much insight into changes in deposition on an altitudinal gradient (de Carvalho and Cavalcanti 2016, Ruijrok et al. 1995). Discrepancies in the amount of eBC_{dry} used in the Col 4 and summit simulations suggest that additional refinement regarding spatial usage of the model must be done in order to better simulate real-world scenarios.

The different eBC_{dry} values used in the Col 4 and summit simulations also led to a difference in M_{eBC}. The summit experienced a higher total M_{eBC} value than the col, despite the higher concentration of eBC_{sub} at the col due the eBC_{dry} value at the summit being over 2 fold of that at the col. However, added melt due to M_t at the col resulted in a larger total melt value at the col than the summit.

In addition to larger amounts of eBC_{dry} at the summit, the lower density of the summit snowpack likely allowed for more M_{eBC} (Table 9) (Marshall 2012). The larger value of M_{eBC} at the summit, due to both larger eBC_{dry} and lower snowpack density, resulted in more

accumulation of eBC on the surface at the summit and thus a higher measured and simulated surface eBC concentrations on day 45 as compared to the col (Marshall 2012).

The larger reduction in albedo at the col, compared to the summit albedo reduction, was likely due to higher eBC_{sub} values at the col. Higher eBC_{sub} values likely caused an increased amount of energy absorption within the snowpack and thus less energy available to be absorbed in the second wave of absorption by LAPs on the surface as well as less energy exiting the entire system.

9.2 Tower Building

9.2.1 Methods

The impact of LAPs on glacial melt can be demonstrated through human modification of surface albedo through the removal of surface impurities. Within a given area, the LAPs on the surface can be cleared off. Over time, the area where surface LAPs have been removed will melt more slowly than the surrounding area that is still contaminated with LAPs (Figure 11). Such formations are modeled by simulating the melt and LAP accumulation for the clean area separately from that of the contaminated area. This is done using 93-day runs in order to simulate the growth of a tower over the entirety of the Cordillera Blanca dry season. In the clean area on day 1, no surface eBC is input into the model. A large dry deposition event of 20,000,000 ng m^{-2} is used to replicate the high amount of LAPs in the still contaminated areas that surround the clean area. The snowmelt

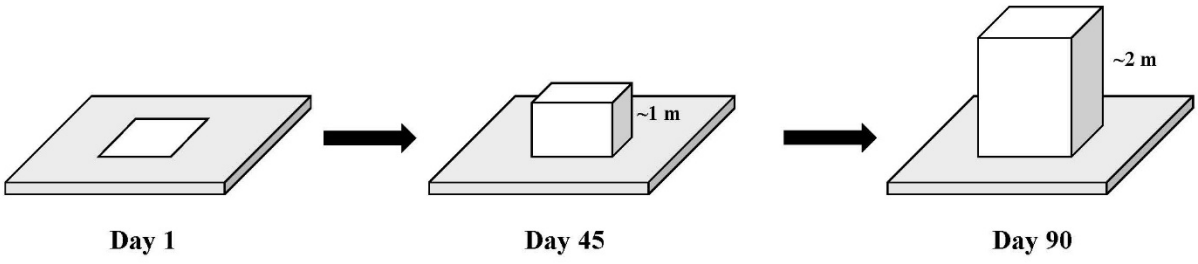

Figure 11: Conceptual model of the growth of a tower over a 90-day period. (Encarnacion et al 2017, unpublished).

due to LAPs and temperature (M_{eBCt}) output on day 93 for the clean area is subtracted from the M_{eBCt} for the contaminated area in order to calculate the forecasted tower height. Simulations for the tower area and the surrounding area were run at 100 m intervals from 4500 to 4900 masl.

9.2.2 Results

The amount of snowmelt in the surrounding and tower areas decreased with altitude for simulations that used an eBC_{sub} concentrations of 10 or 100 ng g^{-1} (Figure 12 a and b), while tower height increased with altitude for both sets of simulations (Figure 12 d and c). Additionally, the surrounding area experienced more melt than the tower area at all altitudes for 10 eBC_{sub} and 100 eBC_{sub}. The maximum amount of snowmelt occurred at 4500 masl for both sets of simulations, but simulations that were run with 100 eBC_{sub} resulted in snowmelt values .56 fold of those that were run with 10 eBC_{sub} (Figure 12 a and b).

Simulations run with 100 eBC_{sub} presented more cumulative melt at all altitudes as compared to simulations that used 10 eBC_{sub}. However, there was a larger discrepancy between the melt values for the surrounding area and the tower for simulations that were run with 10 eBC_{sub} (Figure 12 a), resulting in taller tower heights (Figure 12 c). The tallest tower for simulations that used 10 ng g^{-1} eBC_{sub} was about 2500 mm and 1400 mm for simulations that used 100 ng g^{-1} eBC_{sub} (Figure 12 c and d). Both of these occurred at 4900 masl, and

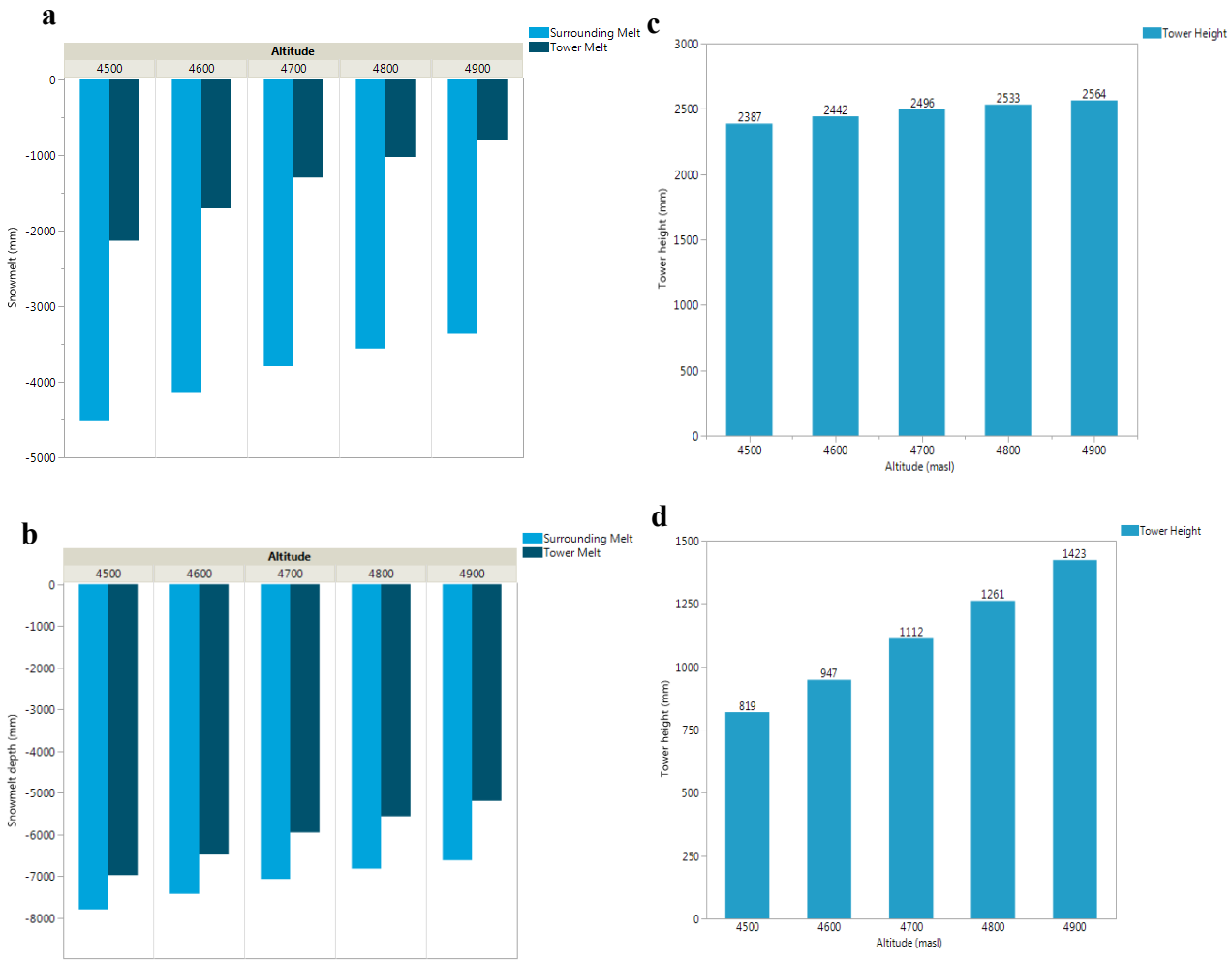

Figure 12: Cumulative snowmelt (mm) of tower areas and their surrounding areas every 100 m between 4500 and 4900 masl with an in-snow eBC concentration of (a) 10 ngg^{-1} and (b) 100 ngg^{-1} and tower heights produced at the same altitudes with an in-snow eBC concentration of (c) 10ngg^{-1} and (d) 100 ngg^{-1}.

tower height decreased as altitude decreased for both sets of simulations (Figure 12 c and d). Additionally, there was a smaller range of tower heights (2387-2564 mm) resulting from simulations run using 10 ng g^{-1} eBC_{sub} as compared to simulations that used 100 eBC_{sub} (819-1423 mm) (Figure 12 c and d).

9.2.3 Discussion

The near 8 meters of estimated snowmelt for simulations using 100 eBC_{sub} has been demonstrated in the Cordillera Blanca in glacier mass balance studies. In an energy and mass balance study conducted by Gurgiser et al. (2013) on Shallap glacier estimated between about 6 m of snow loss between September 2007 and September 2008 and nearly 9 m of snow loss from September 2006 to September 2007 at 4700 masl. At 4800 masl, Gurgiser et al. (2013) estimate between 4 and 6 m of snow loss for the 2007/2008 and 2006/2007 measured years, respectively. This is much lower than the simulated 7 m of snow loss at 4800 m produced by this model. This is likely due to a difference in the integration of temperature in this model as compared to the model constructed and used by Gurgiser et al. (2013).

Additionally, the study found that only 0.17 and 0.18 m of precipitation occurring in the dry season between May and September (Gurgiser et al. 2013). Precipitation is not accounted for in the simulations presented in this study and thus simulated melt does not take into account any gains in mass balance due to precipitation.

Finally, simulated tower heights from simulations that used 10 ng g^{-1} were taller than those run with 100 ng g^{-1} because the smaller concentration of eBC_{sub}. As established in section 8.6, eBC_{sub} had a large impact on the output values for $m_{eBCt,}$ m_{eBC}, M_{eBCt}, and M_{eBC}. Because of the smaller eBC_{sub} value, there is an even larger discrepancy in the drivers of melt

between the tower area and the surrounding areas in simulations that used 10 ng g^{-1} eBC_{sub}. This discrepancy manifests as a larger difference between snowmelt in the surrounding area and snowmelt in the tower area. Despite higher overall amounts of melt for simulations run with 100 ng g^{-1}.

10. Conclusion

The function of the model presented in this study is to assess the impacts of LAPs on the glacial surface and subsurface as well as account for melt due to temperature. This version of the model acts as a stepping stone for further refinement of the operationalization of real-world snowpack processes. Refinement and incorporation of additional processes will increase the accuracy of model simulations. These additions will also allow this model to be incorporated into larger hydrological models with more ease. The incorporation of processes and factors such as sublimation, relative humidity, precipitation events, and vapor pressure are all potential avenues for refinement of the model presented in this study. Additionally, reconstructing the foundations of the model so that it is spatially-based will allow for it to be incorporated into large hydrological models, which are also spatially-based, and further increase our ability to understand and simulate all processes contributing to glacial melt.

Studying glacial melt becomes ever more important as climate change continues to accelerate melt on a global scale. Glaciers act as important water storage units for both human and ecological communities. Beyond the ecological impacts of glacial recession, specifically within the tropics, social and economic structures are threatened by glacial melt (Vergara et al. 2007). In the Cordillera Blanca, the livelihoods of about 80% of the area's population is dependent on subsistence or small-scale agriculture, and thus water resources are essential for household consumption and vocational use (Mark et al. 2010).

Livelihood vulnerability studies indicate that residents of the Cordillera Blanca recognize the ecological and social threats and impacts of glacier recession in the region (Carey 2005, Mark et al. 2010, Bury et al. 2011). Due to the regional population's dependence on subsistence agriculture and livestock grazing, glacier recession threatens food security and household incomes throughout the region (Mark et al. 2010, Bury et al. 2011).

In addition to the agricultural impacts, continual glacial melt in the Cordillera Blanca threatens land stability and massive flooding in the region. In the past there have been many examples in which glacial melt has led to landslides and outburst floods that had major detrimental impacts on local towns (Carey 2005, Hubbard et al. 2005). Outburst floods still pose a major immediate threat to the safety and livelihoods of a larger portion of the population in the Cordillera Blanca (Emmer et al. 2016).

While the focus of this study is tropical glaciers in the Cordillera Blanca, Peru, the model is still applicable to icecaps and sheets at the poles as well as mid-latitude glacial systems. LAPs impact the polar and mid-latitude regions of the cryosphere(Ming et al. 2009, Yasunari et al. 2010, Yasunari et al. 2013, Ginot et al. 2014, Kaspari et al. 2014, Khan et al. 2017), accelerating melt and thus contributing to global sea-level rise. Studying the impacts of LAPs on the cryosphere thus has important implications for our broader understanding of both the ecological and social impacts and implications of climate change.

11. References

Amodio, M., S. Catino, P. Dambruoso, G. De Gennaro, A. Di Gilio, P. Giungato, E. Laiola, A. Marzocca, A. Mazzone, and A. Sardaro. 2014. Atmospheric deposition: sampling procedures, analytical methods, and main recent findings from the scientific literature. Advances in Meteorology **2014**.

Anatolaki, C., and R. Tsitouridou. 2007. Atmospheric deposition of nitrogen, sulfur and chloride in Thessaloniki, Greece. Atmospheric Research **85**:413-428.

Anderson, E. A. 1968. Development and testing of snow pack energy balance equations. Water Resources Research **4**:19-37.

Aoki, T., K. Kuchiki, M. Niwano, Y. Kodama, M. Hosaka, and T. Tanaka. 2011. Physically based snow albedo model for calculating broadband albedos and the solar heating profile in snowpack for general circulation models. Journal of Geophysical Research: Atmospheres **116**.

Babu, S. S., J. P. Chaubey, K. Krishna Moorthy, M. M. Gogoi, S. K. Kompalli, V. Sreekanth, S. Bagare, B. C. Bhatt, V. K. Gaur, and T. P. Prabhu. 2011. High altitude (~ 4520 m amsl) measurements of black carbon aerosols over western trans-Himalayas: Seasonal heterogeneity and source apportionment. Journal of Geophysical Research: Atmospheres **116**.

Bamber, J. L., and A. J. Payne. 2004. Mass balance of the cryosphere. Mass Balance of the Cryosphere, Edited by Jonathan L. Bamber and Antony J. Payne and Foreword by John Houghton, pp. 662. ISBN 0521808952. Cambridge, UK: Cambridge University Press, March 2004.:662.

Bargagli, R., F. Monaci, F. Borghini, F. Bravi, and C. Agnorelli. 2002. Mosses and lichens as biomonitors of trace metals. A comparison study on Hypnum cupressiforme and Parmelia caperata in a former mining district in Italy. Environmental Pollution **116**:279-287.

Barnett, T. P., J. C. Adam, and D. P. Lettenmaier. 2005. Potential impacts of a warming climate on water availability in snow-dominated regions. Nature **438**:303.

Bergknut, M., H. Laudon, S. Jansson, A. Larsson, T. Gocht, and K. Wiberg. 2011. Atmospheric deposition, retention, and stream export of dioxins and PCBs in a pristine boreal catchment. Environmental Pollution **159**:1592-1598.

Blasco, M., C. Domeño, and C. Nerín. 2006. Use of lichens as pollution biomonitors in remote areas: comparison of PAHs extracted from lichens and atmospheric particles sampled in and around the Somport tunnel (Pyrenees). Environmental Science & Technology **40**:6384-6391.

Bradley, R. S., F. T. Keimig, H. F. Diaz, and D. R. Hardy. 2009. Recent changes in freezing level heights in the Tropics with implications for the deglacierization of high mountain regions. Geophysical Research Letters **36**.

Braithwaite, R. J. 1981. On glacier energy balance, ablation, and air temperature. Journal of Glaciology **27**:381-391.

Bury, J. T., B. G. Mark, J. M. McKenzie, A. French, M. Baraer, K. I. Huh, M. A. Z. Luyo, and R. J. G. López. 2011. Glacier recession and human vulnerability in the Yanamarey watershed of the Cordillera Blanca, Peru. Climatic Change **105**:179-206.

Calamari, D., E. Bacci, S. Focardi, C. Gaggi, M. Morosini, and M. Vighi. 1991. Role of plant biomass in the global environmental partitioning of chlorinated hydrocarbons. Environmental Science & Technology **25**:1489-1495.

Cao, Z., Y. Yang, J. Lu, and C. Zhang. 2011. Atmospheric particle characterization, distribution, and deposition in Xi'an, Shaanxi Province, Central China. Environmental Pollution **159**:577-584.

Carey, M. 2005. Living and dying with glaciers: people's historical vulnerability to avalanches and outburst floods in Peru. Global and Planetary Change **47**:122-134.

Castro-Jiménez, J., S. Eisenreich, G. Mariani, H. Skejo, and G. Umlauf. 2012. Monitoring atmospheric levels and deposition of dioxin-like pollutants in sub-alpine Northern Italy. Atmospheric Environment **56**:194-202.

Covert, J. 2015. Impact of the El Niño-Southern Osicllation on Atmospheric Conditions within Tropical Pro-Glacial Valleys. Unpublished.

de Carvalho, L. M. V., and I. F. A. Cavalcanti. 2016. The South American Monsoon System (SAMS). Pages 121-148 *in* L. M. V. de Carvalho and C. Jones, editors. The Monsoons and Climate Change: Observations and Modeling. Springer International Publishing, Cham.

Doherty, S. J., T. C. Grenfell, S. Forsström, D. L. Hegg, R. E. Brandt, and S. G. Warren. 2013. Observed vertical redistribution of black carbon and other insoluble light-absorbing particles in melting snow. Journal of Geophysical Research: Atmospheres **118**:5553-5569.

Emmer, A., J. Klimeš, M. Mergili, V. Vilímek, and A. Cochachin. 2016. 882 lakes of the Cordillera Blanca: an inventory, classification, evolution and assessment of susceptibility to outburst floods. Catena **147**:269-279.

Fang, G.-C., Y.-S. Wu, S.-H. Huang, and J.-Y. Rau. 2004. Dry deposition (downward, upward) concentration study of particulates and heavy metals during daytime, nighttime period at the traffic sampling site of Sha-Lu, Taiwan. Chemosphere **56**:509-518.

Fang, G.-C., Y.-S. Wu, W.-J. Lee, T.-Y. Chou, and I.-C. Lin. 2007. Ambient air particulates, metallic elements, dry deposition and concentrations at Taichung Airport, Taiwan. Atmospheric Research **84**:280-289.

Flanner, M. G., and C. S. Zender. 2005. Snowpack radiative heating: Influence on Tibetan Plateau climate. Geophysical Research Letters **32**.

Flanner, M. G., C. S. Zender, J. T. Randerson, and P. J. Rasch. 2007. Present-day climate forcing and response from black carbon in snow. Journal of Geophysical Research: Atmospheres **112**.

Georges, C. 2004. 20th-Century Glacier Fluctuations in the Tropical Cordillera Blanca, Perú. Arctic, Antarctic, and Alpine Research **36**:100-107.

Ginot, P., M. Dumont, S. Lim, N. Patris, J. D. Taupin, P. Wagnon, A. Gilbert, Y. Arnaud, A. Marinoni, P. Bonasoni, and P. Laj. 2014. A 10 year record of black carbon and dust from a Mera Peak ice core (Nepal): Variability and potential impact on melting of Himalayan glaciers. Cryosphere **8**:1479-1496.

Goelles, T., and C. E. Bøggild. 2017. Albedo reduction of ice caused by dust and black carbon accumulation: a model applied to the K-transect, West Greenland. Journal of Glaciology **63**:1063-1076.

Guo, L.-C., L.-J. Bao, J.-W. She, and E. Y. Zeng. 2014. Significance of wet deposition to removal of atmospheric particulate matter and polycyclic aromatic hydrocarbons: a case study in Guangzhou, China. Atmospheric Environment **83**:136-144.

Gurgiser, W., B. Marzeion, L. Nicholson, M. Ortner, and G. Kaser. 2013. Modeling energy and mass balance of Shallap Glacier, Peru. The Cryosphere **7**:1787-1802.

Hadley, O. L., and T. W. Kirchstetter. 2012. Black-carbon reduction of snow albedo. Nature Climate Change **2**:437-440.

Hicks, B. 1986. Measuring dry deposition: a re-assessment of the state of the art. Pages 75-90 Acidic Precipitation. Springer.

Hock, R. 2003. Temperature index melt modelling in mountain areas. Journal of Hydrology **282**:104-115.

Hubbard, B., A. Heald, J. M. Reynolds, D. Quincey, S. D. Richardson, M. Z. Luyo, N. S. Portilla, and M. J. Hambrey. 2005. Impact of a rock avalanche on a moraine-dammed proglacial lake: Laguna Safuna Alta, Cordillera Blanca, Peru. Earth Surface Processes and Landforms **30**:1251-1264.

Hůnová, I., J. Maznová, and P. Kurfürst. 2014. Trends in atmospheric deposition fluxes of sulphur and nitrogen in Czech Forests. Environmental Pollution **184**:668-675.

Kaser, G., and C. Georges. 1999. On the Mass Balance of Low Latitude Glaciers with Particular Consideration of the Peruvian Cordillera Blanca. Geografiska Annaler. Series A, Physical Geography **81**:643-651.

Kaser, G., I. Juen, C. Georges, J. Gómez, and W. Tamayo. 2003. The impact of glaciers on the runoff and the reconstruction of mass balance history from hydrological data in the tropical Cordillera Blanca, Perú. Journal of Hydrology **282**:130-144.

Kaspari, S., T. H. Painter, M. Gysel, S. M. Skiles, and M. Schwikowski. 2014. Seasonal and elevational variations of black carbon and dust in snow and ice in the Solu-Khumbu, Nepal and estimated radiative forcings. Atmospheric Chemistry and Physics **14**:8089-8103.

Khan, A. L., H. Dierssen, J. P. Schwarz, C. Schmitt, A. Chlus, M. Hermanson, T. H. Painter, and D. M. McKnight. 2017. Impacts of coal dust from an active mine on the spectral reflectance of Arctic surface snow in Svalbard, Norway. Journal of Geophysical Research: Atmospheres **122**:1767-1778.

Kustas, W. P., A. Rango, and R. Uijlenhoet. 1994. A simple energy budget algorithm for the snowmelt runoff model. Water Resources Research **30**:1515-1527.

LaChapelle, E. R. 1969. Field guide to snow crystals. University of Washington Press, Seattle, Book.

Lazarcik, J., J. E. Dibb, A. C. Adolph, J. M. Amante, C. P. Wake, E. Scheuer, M. M. Mineau, and M. R. Albert. 2017. Major fraction of black carbon is flushed from the melting New Hampshire snowpack nearly as quickly as soluble impurities. Journal of Geophysical Research: Atmospheres **122**:537-553.

Mark, B. G., J. Bury, J. M. McKenzie, A. French, and M. Baraer. 2010. Climate Change and Tropical Andean Glacier Recession: Evaluating Hydrologic Changes and Livelihood Vulnerability in the Cordillera Blanca, Peru. Annals of the Association of American Geographers **100**:794-805.

Mark, B. G., and G. O. Seltzer. 2005. Evaluation of recent glacier recession in the Cordillera Blanca, Peru (AD 1962–1999): spatial distribution of mass loss and climatic forcing. Quaternary Science Reviews **24**:2265-2280.

Marshall, S. 2012. The cryosphere. Princeton University Press, Princeton, N.J.

Meador, W., and W. Weaver. 1980. Two-stream approximations to radiative transfer in planetary atmospheres: A unified description of existing methods and a new improvement. Journal of the Atmospheric Sciences **37**:630-643.

Menzies, J. 1995. Modern glacial environments: processes, dynamics, and sediments. Butterworth-Heinemann, Oxford;Boston;.

Ming, J., C. Xiao, H. Cachier, D. Qin, X. Qin, Z. Li, and J. Pu. 2009. Black Carbon (BC) in the snow of glaciers in west China and its potential effects on albedos. Atmospheric Research **92**:114-123.

Odabasi, M., A. Muezzinoglu, and A. Bozlaker. 2002. Ambient concentrations and dry deposition fluxes of trace elements in Izmir, Turkey. Atmospheric Environment **36**:5841-5851.

Oerlemans, J., and J. Fortuin. 1992. Sensitivity of glaciers and small ice caps to greenhouse warming. Science **258**:115-117.

Pacyna, E., J. Pacyna, and N. Pirrone. 2001. European emissions of atmospheric mercury from anthropogenic sources in 1995. Atmospheric Environment **35**:2987-2996.

Paterson, W. S. B. 1994. The physics of glaciers. 3rd edition. Pergamon, Tarrytown, N.Y., U.S.A;Oxford, OX, England;.

Pellicciotti, F., B. Brock, U. Strasser, P. Burlando, M. Funk, and J. Corripio. 2005. An enhanced temperature-index glacier melt model including the shortwave radiation balance: development and testing for Haut Glacier d'Arolla, Switzerland. Journal of Glaciology **51**:573-587.

Petzold, A., J. A. Ogren, M. Fiebig, P. Laj, S. M. Li, U. Baltensperger, T. Holzer-Popp, S. Kinne, G. Pappalardo, N. Sugimoto, C. Wehrli, A. Wiedensohler, and X. Y. Zhang. 2013. Recommendations for reporting "black carbon" measurements. Atmospheric Chemistry and Physics **13**:8365-8379.

Pirrone, N., S. Cinnirella, X. Feng, R. Finkelman, H. Friedli, J. Leaner, R. Mason, A. Mukherjee, G. Stracher, and D. Streets. 2010. Global mercury emissions to the atmosphere from anthropogenic and natural sources. Atmospheric Chemistry and Physics **10**:5951-5964.

Pirrone, N., P. Costa, J. Pacyna, and R. Ferrara. 2001. Mercury emissions to the atmosphere from natural and anthropogenic sources in the Mediterranean region. Atmospheric Environment **35**:2997-3006.

Ruijrok, W., C. I. Davidson, and W. Nicholson. 1995. Dry deposition of particles. Tellus B **47**:587-601.

Sakata, M., Y. Tani, and T. Takagi. 2008. Wet and dry deposition fluxes of trace elements in Tokyo Bay. Atmospheric Environment **42**:5913-5922.

Schauwecker, S., M. Rohrer, D. Acuna, A. Cochachin, L. Davila, H. Frey, C. Giraldez, J. Gomez, C. Huggel, M. Jacques-Coper, E. Loarte, N. Salzmann, and M. Vuille. 2014. Climate trends and glacier retreat in the Cordillera Blanca, Peru, revisited. Global and Planetary Change **119**:85-97.

Schmitt, C. 2018. Thesis Personal Communcation.*in* B. Riggs, editor.

Schneider, S. H., and M. D. Mastrandrea. 2011. Encyclopedia of climate and weather. 2nd edition. Oxford University Press, Oxford;New York;.

Schwarz, J., R. Gao, A. Perring, J. Spackman, and D. Fahey. 2013. Black carbon aerosol size in snow. Scientific reports **3**:1356.

Seinfeld, J. H., and S. N. Pandis. 2006. Atmospheric chemistry and physics: from air pollution to climate change. 2nd edition. J. Wiley, Hoboken, N.J.

Senese, A., M. Maugeri, E. Vuillermoz, C. Smiraglia, and G. Diolaiuti. 2014. Using daily air temperature thresholds to evaluate snow melting occurrence and amount on Alpine glaciers by T-index models: the case study of the Forni Glacier (Italy). The Cryosphere **8**:1921-1933.

Slaymaker, O., and R. E. J. Kelly. 2007. The cryosphere and global environmental change. Blackwell Pub, Malden, MA.

Soriano, A., S. Pallarés, F. Pardo, A. Vicente, T. Sanfeliu, and J. Bech. 2012. Deposition of heavy metals from particulate settleable matter in soils of an industrialised area. Journal of Geochemical Exploration **113**:36-44.

Teil, M.-J., M. Blanchard, and M. Chevreuil. 2004. Atmospheric deposition of organochlorines (PCBs and pesticides) in northern France. Chemosphere **55**:501-514.

Thomas, J. L., C. M. Polashenski, A. J. Soja, L. Marelle, K. A. Casey, H. D. Choi, J. C. Raut, C. Wiedinmyer, L. K. Emmons, J. D. Fast, J. Pelon, K. S. Law, M. G. Flanner, and J. E. Dibb. 2017. Quantifying black carbon deposition over the Greenland ice sheet from forest fires in Canada. Geophysical Research Letters **44**:7965-7974.

Toon, O. B., C. McKay, T. Ackerman, and K. Santhanam. 1989. Rapid calculation of radiative heating rates and photodissociation rates in inhomogeneous multiple scattering atmospheres. Journal of Geophysical Research: Atmospheres **94**:16287-16301.

Vassura, I., F. Passarini, L. Ferroni, E. Bernardi, and L. Morselli. 2011. PCDD/Fs atmospheric deposition fluxes and soil contamination close to a municipal solid waste incinerator. Chemosphere **83**:1366-1373.

Vergara, W., A. Deeb, A. Valencia, R. Bradley, B. Francou, A. Zarzar, A. Grünwaldt, and S. Haeussling. 2007. Economic impacts of rapid glacier retreat in the Andes. Eos, Transactions American Geophysical Union **88**:261-264.

Vuille, M., and R. S. Bradley. 2000. Mean annual temperature trends and their vertical structure in the tropical Andes. Geophysical Research Letters **27**:3885-3888.

Vuille, M., R. S. Bradley, M. Werner, and F. Keimig. 2003. 20th century climate change in the tropical Andes: observations and model results. Pages 75-99 Climate variability and change in high elevation regions: past, present & future. Springer.

Vuille, M., B. Francou, P. Wagnon, I. Juen, G. Kaser, B. G. Mark, and R. S. Bradley. 2008a. Climate change and tropical Andean glaciers: Past, present and future. Earth-science reviews **89**:79-96.

Vuille, M., G. Kaser, and I. Juen. 2008b. Glacier mass balance variability in the Cordillera Blanca, Peru and its relationship with climate and the large-scale circulation. Global and Planetary Change **62**:14-28.

Wagnon, P., P. Ribstein, B. Francou, and B. Pouyaud. 1999a. Annual cycle of energy balance of Zongo glacier, Cordillera Real, Bolivia. Journal of Geophysical Research: Atmospheres **104**:3907-3923.

Wagnon, P., P. Ribstein, G. Kaser, and P. Berton. 1999b. Energy balance and runoff seasonality of a Bolivian glacier. Global and Planetary Change **22**:49-58.

Wiscombe, W. J., and S. G. Warren. 1980. A model for the spectral albedo of snow. I: Pure snow. Journal of the Atmospheric Sciences **37**:2712-2733.

Wu, S., S. Tao, F. Xu, R. Dawson, T. Lan, B. Li, and J. Cao. 2005. Polycyclic aromatic hydrocarbons in dustfall in Tianjin, China. Science of the Total Environment **345**:115-126.

Xu, B., J. Cao, J. Hansen, T. Yao, D. R. Joswia, N. Wang, G. Wu, M. Wang, H. Zhao, and W. Yang. 2009. Black soot and the survival of Tibetan glaciers. Proceedings of the National Academy of Sciences **106**:22114-22118.

Xu, B., J. Cao, D. R. Joswiak, X. Liu, H. Zhao, and J. He. 2012. Post-depositional enrichment of black soot in snow-pack and accelerated melting of Tibetan glaciers. Environmental Research Letters **7**:014022.

Yasunari, T. J., P. Bonasoni, P. Laj, K. Fujita, E. Vuillermoz, A. Marinoni, P. Cristofanelli, R. Duchi, G. Tartari, and K. M. Lau. 2010. Estimated impact of black carbon deposition during pre-monsoon season from Nepal Climate Observatory - Pyramid data and snow albedo changes over Himalayan glaciers. Atmospheric Chemistry and Physics **10**:6603-6615.

Yasunari, T. J., Q. Tan, K.-M. Lau, P. Bonasoni, A. Marinoni, P. Laj, M. Ménégoz, T. Takemura, and M. Chin. 2013. Estimated range of black carbon dry deposition and the related snow albedo reduction over Himalayan glaciers during dry pre-monsoon periods. Atmospheric Environment **78**:259-267.

12. Appendix A: Extended Methods

12.1 Light Absorbing Heating Method (LAHM) Instrument

The instrument used in this method is designed to determine particle properties of particles on 25mm diameter filters, however configurations for other filter size are possible. The instrument is composed of several plexiglass sheets 25x25 cm in size. The bottom sheet of plexiglass is 2cm thick and has a 23 mm diameter that goes 1.5 cm into the sheet. The remaining 0.5 cm is drilled to the size of the infrared thermometer module (approximately 0.8 cm diameter). The infrared thermometer module (MELEXIS MLX90614ESF-BAA-000-TU-ND non-contact infrared thermometer for use with Arduino) is secured on the bottom of the sheet which is them secured onto the instrument base with space for the module board and the wires. For analysis, a 25 mm filter is placed over the 23 mm hole which places the bulk of the filter bottom in the field of view of the infrared thermometer. Two additional plexiglass sheets with holes of incr easing diameter size are placed on top of the first sheet for the analysis process. To prevent the accumulation of warmed air above the filter, a gap is created using two 2.5x2.5 cm sheets 0.5 cm thick and a final 25x25 cm sheet 0.5 cm thick again. An LED light (PHILIPS 50W replacement indoor flood model number: BC7PAR16, 9290012454) is then placed onto four small rubber bumpers on top of the final sheet, again, to prevent direct heat transfer from the bulb to the instrument. The final configuration was determined through experimentations in an effort to reduce heat exchange between components of the instrument, The infrared module is operated by an Arduino microcontroller which also controls the light through a commercially available relay system, the PowerSwitch tail II.

An Arduino program has been written to operate the system through five illumination and cooling cycles. Averaged data produce an extremely stable signal. The first four

illumination periods are 30 seconds and the final is 120 seconds, all with 90 seconds cooling periods in between. The instrument has thus far been used only for 25 mm filters investigating light absorbing particles on glaciers. Therefore, results and calibration are focused on 25 mm filters.

6.3.2 Instrument Calibration

Basic instrument calibration has been completed using specially prepared Millipore 0.22 micron filters (GSWP02500 Mixed Cellulose Ester Filter Membrane) and laboratory grade fullerene soot (Baumgardner et al., xxx). Mixtures of fullerene soot in water were created enabling a known amount of fullerene soot to be deposited onto the filters **(Schmitt et al., 2015)**. The temperature traces were normalized by subtracting the temperature of the ten seconds prior to illumination. In total, approximately 50 calibration filters have been created, with fullerene soot masses ranging from 1.0 microgram to 100 micrograms. The following equation shows the functional fit relating temperature increase to micrograms of soot:

$$M = 0.395 * T^2 - 0.326 * T + 0.792$$

where M is the mass in micrograms and T is the temperature increase in degrees C.

13. Appendix B: Extended Background

13.1. Climate of the Cordillera Blanca

The Cordillera Blanca, situated between 8ºS and 10ºS in the Ancash region of Peru, is a subsection of the greater Andes mountain range and the most glaciated tropical region in the world. The range is 180 kilometers long and 20 kilometers at its widest point, with an elevation range from 3,000-6,768 meters above sea level (masl). As in most of the central Andes, the Cordillera Blanca separates the dry Pacific slope from the wet Amazon basin. Most of the precipitation in the region originates from easterly winds which carry moisture from Amazon basin. The wet season takes place during the austral summer and the dry season spans from May to September. Approximately 70-80% of the total yearly precipitation in the Cordillera Blanca takes place during the wet season.

13.1.1 El Niño-Southern Oscillation

The El Niño-Southern Oscillation (ENSO) is a major climate event that heavily influences semiannual precipitation rates in the Cordillera Blanca, and the entirety of the South American continent. ENSO links changes in atmospheric patterns cause by the Southern Oscillation along with large scale fluctuations of ocean surface temperatures of the tropical Pacific driven by El Nino that generate wide spread climatic changes every 2-7 years.

During El Niño above-average off-shore sea surface temperatures (SSTs) arise off of the west coast of South America in the Pacific between March and May. Along with such changes in the ocean, the Southern Oscillation causes atmospheric fluctuations of The Intertropical Convergence Zone (ITCZ), a narrow band of rising air, cloudiness, and high rainfall in the eastern Pacific. The rising air in the ITCZ occurs from Hadley cells in the lower atmosphere, where the convective area of the cells are located near the equator

(Schneider and Mastrandrea 2011). During El Nino cycles the ITCZ moves to or south of the equator which causes an array of changes throughout the Pacific including weakened trade winds and a region of unusually high amounts of precipitation near the dateline.

In the mature phase of ENSO, weak trade winds cover most of the Pacific, caused by the southward shift of the ITCZ, and high SSTs. This creates higher rates of heat transfer from the ocean into the atmosphere, causing most of the troposphere over the Pacific to be incredibly warm. In turn, the warmer temperatures of troposphere maintain the high precipitation patterns until SST declines in the eastern Pacific. From these weak trade wind patterns and high SSTs, the thermocline, the interface between the warm surface water and cold, denser water, deepens. The SST anomaly first appears off of the coast of Peru when the cold Humboldt current is capped by the newly present warm water.

In the Cordillera Blanca, ENSO regulates precipitation, humidity, and air temperature, all of which impact glacier mass balance. In El Niño years, mass balance is typically negative as compared to average because the atmosphere situated over the eastern tropical Pacific is dry and cold. During this time the western tropical Pacific experiences low sea-pressure and the atmosphere is warm, generating large amounts of precipitation in the west. However, La Niña causes above average mass balance in the Cordillera Blanca because the zone of warm air and high rates of precipitation move eastward due to a relaxation of the trade winds (Vuille et al. 2008b). On the microclimate scale, or in individual valleys within the Cordillera Blanca, similar regional impacts of ENSO are felt, but various elements of the event are reduced or muted within these microclimates (Covert 2015).

13.1.2 The South American Monsoon System

The South American Monsoon System (SAMS) is an additional major climatic event that heavily impacts the climate of the South American continent and the Cordillera Blanca. The main driver of the SAMS cycle is the difference in heating between the Atlantic Ocean and the South American landmass (de Carvalho and Cavalcanti 2016). SAMS largely contributes to the stark contrast of precipitation rates between the wet versus dry season in the Cordillera Blanca. The largest contrasts between summer and winter precipitation occurs in the Central Amazon at 10°S with almost all precipitation falling in the summer months. This large contrast in precipitation amounts in the central Amazon influences precipitation patterns in the Cordillera Blanca because the range is also at 10ºS.

13.1.3 Other Influential Climatic Patterns

While SAMS drives high levels of moisture on the eastern slope of the Cordillera Blanca, other climatic features such as the Humboldt Current, atmospheric Walker circulation, and prevailing wind surfaces create the dry climate on the western slope of the range. The Humboldt Current, brings cold water from the Antarctic south Pacific up the coast of South America. Prevailing winds from southeast Pacific and Walker circulation both bring cold air to the western coast of South America. The combination of these three climatic elements create the dry climate seen on the western slope of the Cordillera Blanca, and the Peruvian Andes in general.

13.1.4 Climate Change in the Cordillera Blanca

The warming trend in the Cordillera Blanca has doubled in the last 40 years and tripled in the last 25 years (Vuille and Bradley 2000). The average minimum temperature, calculated from data from over 30 stations on mountains situated throughout the entirety of the region, in the Cordillera Blanca has increased by 0.29ºC per decade (from 1983-2012)

while the mean maximum temperature has decreased by 0.04ºC per decade over the same time period (Schauwecker et al. 2014). Overall, there has been a reported increase of 0.35-0.39°C/decade from 1951 to 1999 (Mark and Seltzer 2005). Over time, the minimum and maximum temperatures with continue to diverge and impact the ratio of accumulation to ablation, which in turn heavily affects glacier mass balance in the Cordillera Blanca (Marshall 2012). Additionally, climate change has heavily impacted glacier accumulation and ablation which are the two largest drivers of glacier mass balance.

13.2 Pollutant Types Extended

Table 10: Recommendations for reporting types of black carbon based on properties and techniques used in studies (Petzold et al., 2013).

Property	Technique	Instrument	Reported Value	Recommendation
Light absorption	Light absorption measurement	Various in-situ and filter-based methods Photoacoustic Spec. Aethalometer MAAP PSAP COSMOS	Light absorption coefficient σ_{ap}; mass concentration computed from σ_{ap} by applying a specific mass absorption cross-section MAC	Report as σ_{ap}; If reported as EBC, specify MAC value used for the conversion from light-absorption into mass concentration
Refractory	Measurement of thermal radiation	SP2 LII	Mass concentration	Report as rBC Specify means of calibration, conversion factor from thermal radiation to carbon mass, and the size-cut of rBC particles
	Soot Particle Aerosol Mass Spectrometry	SP-AMS	Mass concentration OC/rBC mass fraction	Report as rBC
Chemical composition, carbon content	Evolved carbon methods, thermal evolution of carbon with optical correction for pyrolysis	Various temperature protocols	Mass concentration OC/EC mass fraction	Report as EC; Specify temperature protocol used for the sample analysis
	Aerosol Time-of Flight Mass Spectrometry	ATOFMS SP_AMS	Mass concentration OC/EC mass concentration	Report as EC Report as rBC, because technique detects carbon that is evaporating under incandescent conditions
	Soot Particle Aerosol Spectrometry		Mass concentration OC/rBC mass fraction	
Graphite-like microstructure	Raman spectrometry		Mass concentration	Report as EC, Specify means of calibration
Particle morphology	Electron Microscopy		Structural information	Not applicable

13.3 Key Terms

All definitions are taken from Marshall (2012).

(Glacial) Ablation: all processes in which snow or ice is lost from the glacier. These include but are not limited to snow or ice melt, calving events, sublimation, ice fall and avalanches.

Accumulation: all processes that incorporate material to the glacier. Materials include snow or ice as well as atmospheric particles. These include but are not limited to precipitation events, atmospheric deposition of pollutants, and densification (ice).

Albedo: the fraction of incoming radiation that is reflected back off of a surface.

Light Absorbing Particles (LAP): generally any particulate matter with a grain diameter of 0.7 microns or greater that are deposited on a glacial surface or incorporated within the snowpack.

Mass Absorption Cross Section: the ratio of an area that is covered by light absorbing particles. The area covered by such particles is assumed to be one hundred percent absorptive.

Mass Balance: the difference between accumulation and ablation on a glacier.

Surface Energy Balance: the energy processes that govern the amount of energy that is available for ablation of a glacier. Such processes include solar radiation, sensible heat flux, latent heat flux, ablation, and accumulation.

Appendix C: Figures and Tables

Table 11: Simulated surface eBC values for Pisco and Vallunaraju on day 1 and day 93 for altitudes every 100 m between 4700 and 5700 masl.

Mountain	Altitude (masl)	Day 1 sim eBC	Day 93 sim eBC	Day 1 total eBC	Day 93 total eBC	Day 1 albedo	Day 93 albedo
Pisco							
	4700	10	1766.09	0	10,536,556.91	0.78	0.71
	4800	10	1422.4	0	8,474,380.36	0.78	0.72
	4900	10	1137.48	0	6,764,879.46	0.78	0.73
	5000	10	901.48	0	5,348,884.16	0.78	0.74
	5100	10	694.31	0	4,105,834.09	0.78	0.75
	5200	10	515.27	0	3,031,613.05	0.78	0.76
	5300	10	380.62	0	2,223,717.74	0.78	0.77
	5400	10	288.95	0	1,673,723.60	0.78	0.77
	5500	10	268.93	0	1,553,583.46	0.78	0.77
	5600	10	268.93	0	1,553,583.46	0.78	0.77
	5700	10	268.93	0	1,553,583.46	0.78	0.77
Vallunaraju							
	4700	30	12006.31	0	71,857,875.46	0.78	0.40
	4800	30	9972.16	0	59,652,959.24	0.78	0.45
	4900	30	8244.02	0	49,284,112.1	0.78	0.49
	5000	30	6780.4	0	40,502,414.4	0.78	0.53
	5100	30	5468.97	0	32,633,821.59	0.78	0.57
	5200	30	4313.75	0	25,702,488.83	0.78	0.61
	5300	30	3430.46	0	20,402,730.55	0.78	0.64
	5400	30	2821.55	0	16,749,325.4	0.78	0.67
	5500	30	2687.7	0	15,946,180.07	0.78	0.67
	5600	30	2687.7	0	15,946,180.07	0.78	0.67
	5700	30	2687.7	0	15,946,180.07	0.78	0.67